Journal of Structural Geology 137 (2020) 104082

Contents lists available at ScienceDirect

Journal of Structural Geology

journal homepage: http://www.elsevier.com/locate/jsg

Deformation mechanics in inclined, brittle-ductile transpression zones: Insights from 3D finite element modelling

Seyed Tohid Nabavi [a,*], Seyed Ahmad Alavi [a], Manuel Díaz-Azpiroz [b], Soheil Mohammadi [c], Mohammad Reza Ghassemi [d], Carlos Fernández [e], Leticia Barcos [b], Marcel Frehner [f]

[a] Faculty of Earth Sciences, Department of Geology, Shahid Beheshti University, Tehran, Iran
[b] Departamento Sistemas Físicos, Químicos y Naturales, Universidad Pablo de Olavide, Crtra, Utrera, Km 1, 41013, Seville, Spain
[c] High Performance Computing Laboratory, School of Civil Engineering, University of Tehran, Tehran, Iran
[d] Research Institute for Earth Sciences, Geological Survey of Iran, Tehran, Iran
[e] Departamento de Ciencias de La Tierra, Universidad de Huelva, Campus de El Carmen, 21071, Huelva, Spain
[f] Zurich University of Teacher Education (PHZH), Zurich, Switzerland

ARTICLE INFO

Keywords:
Oblique convergence
Inclined transpression
Inclined extrusion
Strain partitioning
3D finite-element modelling

ABSTRACT

Most natural examples of transpression zones developed at oblique convergence regime are inherently 3D and have inclined boundaries. A 3D finite element model with an elasto-plastic rheology is used to investigate the structural and mechanical evolution of inclined transpression zones in a rock sequence above a frictional basal detachment. Inelastic constitutive relationships allow permanent strains to develop in response to the applied loads. FE-modelling results show that oblique convergence is accommodated by discrete deformation at the main pre-existing inclined faults (=70°) and by distributed brittle and ductile deformation at active blocks. Oblique contraction at the active blocks resulted mainly in layer-parallel shortening, orthogonal to the model outer boundaries, whereas thickening in the horizontal and vertical directions was accommodated via layer-parallel, fault strike-parallel extension and up-dip extrusion (i.e., inclined extrusion). Lateral extrusion should have compensated the rest and/or volume loss took place. Folding and thickening of the mobile backstop produced a non-cylindrical, asymmetric, bi-vergent anticline where permanent strains developed principally in the steep forelimb. Secondary, conjugate fault zones also accommodate oblique slip and contribute to uplift. Displacement vectors within the transpression zone are rotated counter-clockwise (ca. 20°–30°) with respect to vectors in the fixed backstop. Areas with higher rotation values seem to correlate with those showing higher ellipticity values. The presence of pre-existing faults favored strain partitioning from the onset of deformation. FE-modelling results compared with analytical, natural example, and analogue modelling results show that our mechanical modelling can overall match inclined transpression zones geometry that present different modes of strain partitioning and localisation.

1. Introduction

Transpression (and transtension) kinematics derives from obliquity between velocity vectors and boundaries between deforming crustal blocks, an inevitable consequence of the rotational character of plate tectonics (Harland, 1971; Dewey et al., 1998; Díaz-Azpiroz et al., 2016; Philippon and Corti, 2016). Oblique convergence produces transpressional deformation in many different tectonic settings, including fold-and-thrust belts (e.g., Sarkarinejad et al., 2013; Barcos et al., 2015; Li et al., 2018), mountain ranges (e.g., Nabavi et al., 2017b; Malavieille et al., 2019), accretionary wedges (e.g., Schulmann and Gayer, 2000) or intraplate deformation zones (e.g., Bradley et al., 2017; van Gelder et al., 2017). Kinematically, transpression zones form from the simultaneous operation of two components, simple shearing and coaxial flow (Fossen and Tikoff, 1993; Fernández and Díaz-Azpiroz, 2009; Frehner, 2016; Fossen and Cavalcante, 2017) resulting in non-plane strain. In this regard, the study of transpression (and transtension) zones helps us to better understand crustal 3D kinematics, as deduced from many field-based studies (e.g., Díaz-Azpiroz and Fernández, 2005; Zanchi et al., 2016; Nabavi et al., 2017b, 2017c; Simonetti et al., 2018; Bergh et al., 2019; Alonso-Henar et al., 2020), as well as analytical (e.g., Fossen et al., 1994; Fossen and Tikoff, 1998; Jones et al., 2004; Jiang, 2007;

* Corresponding author. Faculty of Earth Sciences, Department of Geology, Shahid Beheshti University, Tehran, Iran. Tel.: +989112914581
E-mail addresses: tohidnabavi@gmail.com, T_nabavi@sbu.ac.ir (S.T. Nabavi).

https://doi.org/10.1016/j.jsg.2020.104082
Received 15 October 2019; Received in revised form 27 April 2020; Accepted 27 April 2020
Available online 11 May 2020

Fernández and Díaz-Azpiroz, 2009; Díaz-Azpiroz et al., 2019) (Fig. 1), analogue (e.g., Tikoff and Peterson, 1998; Casas et al., 2001; Leever et al., 2011; Ghosh et al., 2014; Barcos et al., 2016; Sadeghi et al., 2016), and numerical (e.g., Davis et al., 2013; Nevitt et al., 2014, 2017; Dasgupta et al., 2015; Frehner, 2016; Nabavi et al., 2017a, 2018a, 2018b, 2019) models. In essentially ductile transpressional zones both simple shearing and coaxial flow are commonly present within the entire shear zone producing complex finite deformation geometries (e.g., Alsop et al., 1998; Vitale and Mazzoli, 2008, 2015; Davis and Titus, 2011; Fernández et al., 2013; Fossen and Cavalcante, 2017; Carreras and Druguet, 2019). In contrast, brittle-ductile shear zones usually show significant strain partitioning producing separate, large-scale deformational domains characterized by different kinematics (Tikoff and Teyssier, 1994; Curtis, 1998; Schulmann et al., 2003; Jones et al., 2005).

Some natural shear zones have monoclinic symmetries, with strike- and/or dip-parallel lineations. However, many other cases have variably oriented oblique lineations (e.g., Hudleston et al., 1988; Sullivan and Law, 2007), which cannot be explained by monoclinic models. Such shear zones are more realistically modelled by transpression with triclinic symmetry (e.g., Robin and Cruden, 1994; Lin et al., 1998; Czeck and Hudleston, 2003, 2004; Iacopini et al., 2007; Horsman et al., 2008; Fernández and Díaz-Azpiroz, 2009; Viola and Henderson, 2010; Toy et al., 2013; Xypolias et al., 2018). Triclinic transpression can be reproduced by horizontal velocity vectors acting on inclined shear zone boundaries, which was termed 'inclined transpression' (Dutton, 1997), and can be depicted in a 'strain triangle' (Jones et al., 2004; Díaz-Azpiroz et al., 2014).

Moreover, most oblique convergence settings are horizontally and vertically heterogeneous in their constitutive properties, which affect the structural style and deformation mechanics. Therefore, the structural style and fault systems patterns in natural transpressive (or transtensional) zones are controlled, in addition to the convergence angle, by the orientation of the mechanical layering with respect to the strain field, the relative orientation of pre-existing faults, and the coefficient of sliding friction on the fault plane (Bott, 1959; Hughes et al., 2014; Hughes and Shaw, 2015; Ferrill et al., 2017; Nabavi et al., 2017a, 2018a). Mechanical stratigraphy causes non-uniform deformation of multilayer systems when subjected to tectonic stress (e.g., Treagus, 1993; Gomez-Rivas and Griera, 2012). Mechanical stratigraphy contains different ranges of material heterogeneity and anisotropy such as layered units (competent and incompetent layers), the presence of bedding-plane discontinuities (Cooke and Underwood, 2001; Bourne, 2003; Bose et al., 2018), the thicknesses of the mechanical layers, tensile strengths (range from 2 to 40 MPa, Bieniawski, 1984), the compressive strengths (from 30 to 350 MPa, Bieniawski, 1984), the Young's modulus (from about 1 to 100 GPa, Eschbac, 1961; Byerlee, 1970), the character and frictional properties of the transitions or, the confining stress at the brittle and ductile deformation (range between 30 and 300 MPa, Jaeger et al., 2007). These factors cause the wide range of geological structures and influence on their evolution (e.g., fold formation, failure mode, fault geometry and growth, spacing of fractures/faults, displacement distribution and gradient, dip of slip surfaces, fault zones width, etc.; see McClay et al., 2004; Ferrill and Morris, 2008; Ferrill et al., 2017; Michie et al., 2014; McGinnis et al., 2016; Boersma et al., 2020).

In this study, we present, for the first time, a non-linear 3D FE-model that simulates the deformation mechanics in an inclined (thus triclinic) transpression zone affecting an alternating brittle-ductile-brittle sedimentary cover frictionally detached from a competent rock basement. In addition, it is important to note that we use non-rigid deformation zone boundaries and backstops. The terminology used to convey the lithostratigraphic influence on structural style includes lithotectonic units and structural-lithic units (Woodward and Rutherford, 1989). The presented model is purposely simplistic. Geological processes, such as diagenesis, erosion, fluid flow, temperature, etc. are not considered. The primary reason for this approach is that we seek to isolate the effects of a few selected parameters, such as material properties, oblique convergence and fault geometry in order to keep the analysis tractable. While the effect of additional processes could be investigated, they would produce a wide range of even more complex structural geometries, and thus would increase the difficulties in providing unambiguous interpretations of the results.

Our results are focused on (1) geometry, kinematics, and mechanics of structural deformation, (2) variation of slip along fault segments, and (3) spatial variation of the displacement vectors, so that we attempt to address: (i) the importance of oblique convergence in the deformation patterns of inclined transpression developed in upper crustal conditions

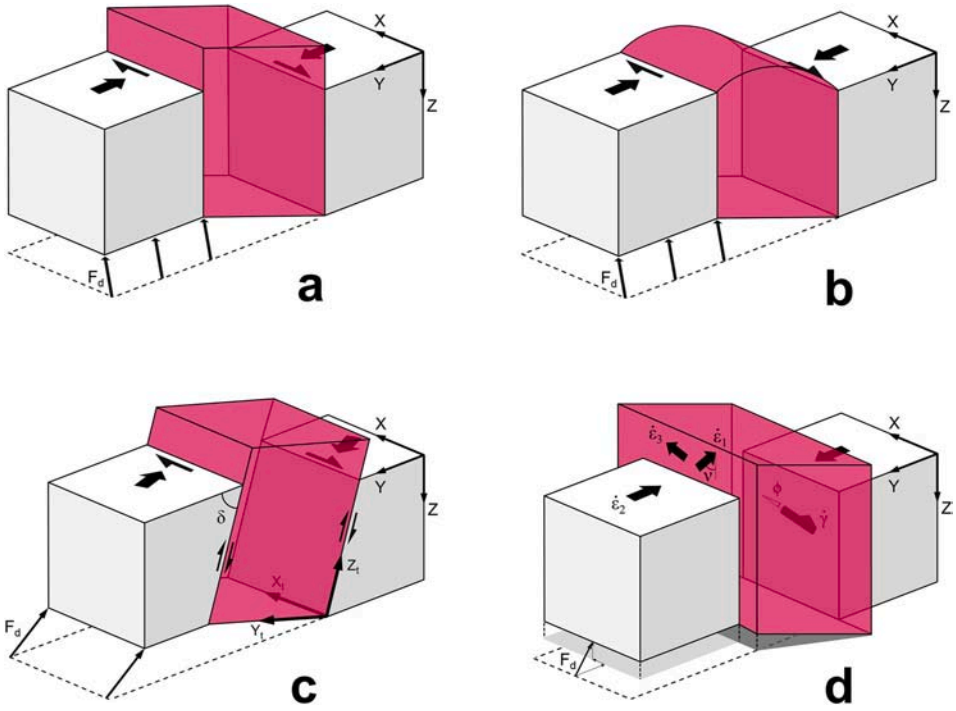

Fig. 1. Models of transpression zones mentioned in the text. Reference frame: X is horizontal and parallel to the strike of the transpression zone boundary; Y is horizontal and normal to the transpression zone boundary; and Z is vertical. F_d is the convergence vector between the zone-bounding blocks. a) Classical model of monoclinic transpression zone (Sanderson and Marchini, 1984; Fossen and Tikoff, 1993). b) Transpression zone model with no-slip boundaries (Robin and Cruden, 1994; Dutton, 1997). c) Inclined transpression kinematic model (Jones et al., 2004). The reference coordinate system, X_t, Y_t, and Z_t is fixed to the shear zone and differs from the far-field coordinate system X, Y, Z. δ is the dip of the zone boundaries. d) Model of triclinic transpression with oblique simple shear and inclined extrusion direction (Fernández and Díaz-Azpiroz, 2009). Transpression obliquity φ is the angle between the simple shearing direction and the strike of the transpression zone. $\dot{\gamma}$ is simple shear strain rate. $\dot{\varepsilon}_1$, $\dot{\varepsilon}_2$ and $\dot{\varepsilon}_3$ are strain rates. Extrusion obliquity ν is the angle between the extrusion direction ($\dot{\varepsilon}_1$) and the dip of the transpression zone.

(with frictional detachment and plastic interlayers), (ii) the influence of mechanical stratigraphy in the construction of the transpression zone, (iii) the possible trends for strain refraction across different layers in the transpression zone, (iv) the implications of strain results in the prediction and development of probable brittle and ductile structures within the transpression zone, and (v) the effects of inherited structures in the strain partitioning and the geometry of the resulting wedge. In the discussion section, insights from FE-model results in strain partitioning are investigated and linked to the analytical, kinematic, analogue, and numerical models established before. Our approach is general; hence, its conclusions are independent from the specific structural geometry and can be then applied to other examples and tectonic settings.

2. Model setup

The numerical model is based on the concept of continuum

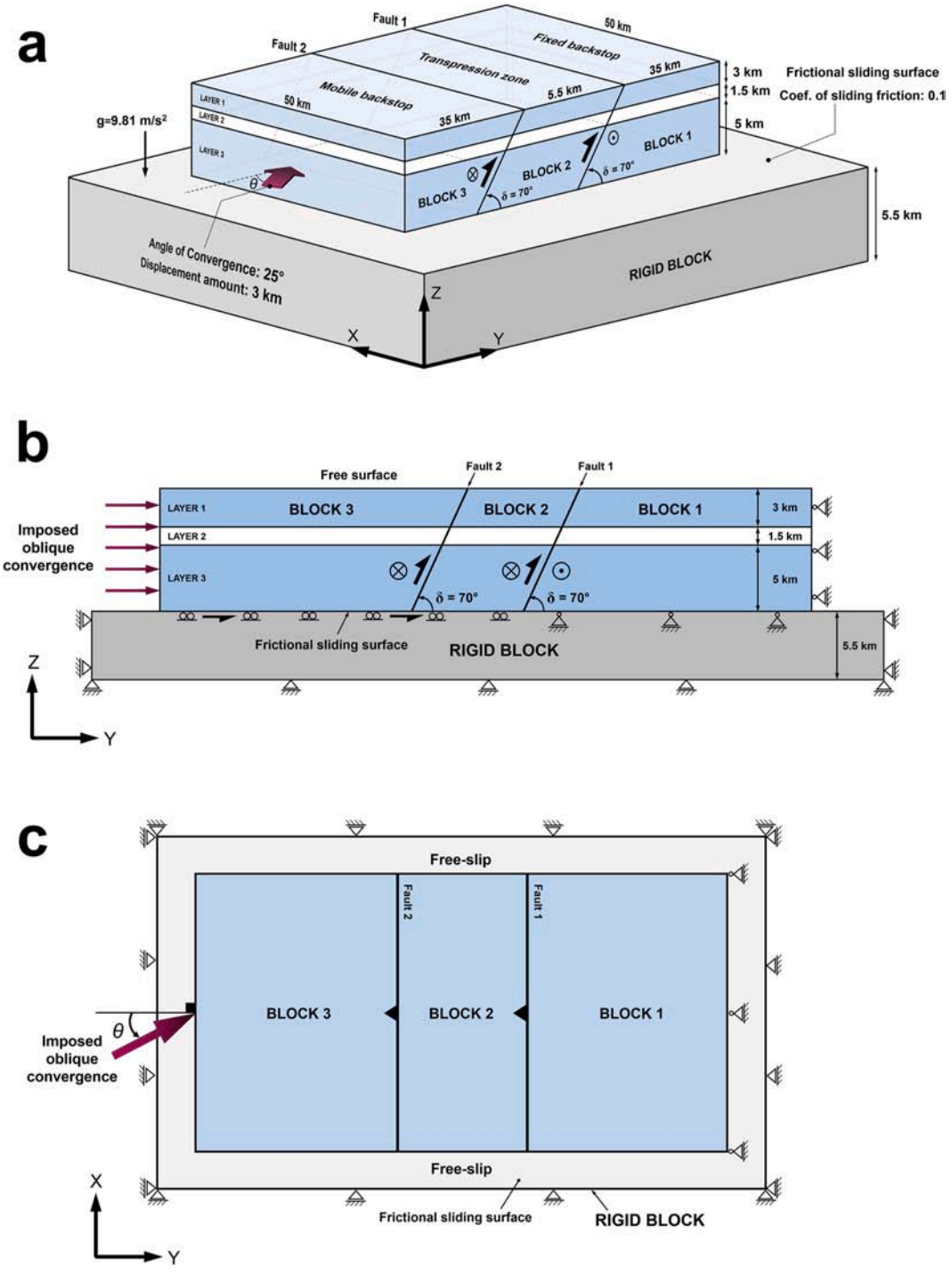

Fig. 2. Initial setup of the three-dimensional FE-model: a) Three-dimensional block diagram; b) cross-sectional view (YZ-plane); and c) map view (XY-plane) of the model showing the imposed load, boundary conditions, and rheology of mechanical layering. Boundary conditions are no-slip at the right side and at the bottom of block 1, constant oblique convergence in the horizontal direction at the left side and at the bottom of blocks 2 and 3; and free surface at the top boundary. The free surface boundary condition at the top model face allow self-consistent evolution of topography. In addition, both lateral boundary conditions are defined as free-slip along the boundary planes. Finally, the study model is discretised to 15,032 three-dimensional 8-node elements.

mechanics and the governing system of partial differential equations is solved numerically with the finite element method. The general purpose FE-ABAQUS™ commercial code (ABAQUS/CAE; FE-commercial program ABAQUS™ tutorial version 6.14–2, 2014; www.simulia.com/) was selected for this study because it is well suited to analyse geomechanical problems over a wide range of scales in 1, 2, and 3D. ABAQUS™ employs a Lagrangian formulation that accurately handles large strains and rotations as well as complex contact interfaces with frictional behaviour where significant sliding can occur. It also has efficient algorithms for solving highly non-linear problems that result from both geometric complexity and material behaviour. In addition, ABAQUS™ has a large flexibility of model constitutive relationships that are appropriate for simulating the behaviour of rocks, ranging from simple elastic material models to advanced elastic-plastic (e.g., Mohr-Coulomb, Drucker-Prager, Damage mechanics) and visco-elastic material models.

The proposed model (Fig. 2) comprises an upper, three-layered block that slides frictionally on top of a rigid basement. The upper block is segmented by two dipping, parallel fault planes into three blocks, which are called here 'active' blocks. The coordinate system is defined by a horizontal XY plane, with the X-axis parallel to the strike of the fault planes, and a vertical Z-axis (Fig. 2a). The rigid block is 5.5 km thick whereas the upper, middle, and lower layers of the 'active' blocks are 3, 1.5 and 5 km thick, respectively (Fig. 2a and b). The lateral dimensions of the 'active' block are 75.5 × 50 × 9.5 km and the two faults, planar and mutually parallel, are 50 km long, dip 70° and end at tip lines (Fig. 2a and b). Additionally, the sidewalls and the upper surface were unhindered, so that displacement along the fault planes is allowed both horizontally (along the X-axis) and up-dip (Y- and Z-axis), thus resulting in oblique-slip faults in the analysis. These faults were simulated with frictional sliding interfaces that employ a classic Mohr-Coulomb friction model, with a 0.6 friction coefficient assigned to the fault interfaces. The deforming material between faults is allowed to shorten (or lengthen), and shear vertically and horizontally.

The rheology of the upper crust is elasto-plastic, which means that stresses increase with strain up to a certain limit, where failure occurs and plastic deformation starts. Furthermore, elasto-plastic models usually provide the most reliable representations of shallow faulting behaviour. In this regard, an elasto-plastic constitutive law was implemented with the elastic component assumed to be linear isotropic by assigning Mohr-Coulomb plasticity. This constitutive definition introduced six model parameters into the analysis: Young's modulus (E), Poisson's ratio (υ), gravitational acceleration (g), rock cohesion (C), rock internal friction (φ), and basal friction (μ). The material properties of the three active block layers are, from up to bottom, elasto-plastic limestones with an elastic modulus of 48 GPa, a Poisson ratio of 0.25, and a density of 2700 kg/m^3, plastic marls with an elastic modulus of 0.2 GPa, a Poisson ratio of 0.2, and a density of 2100 kg/m^3, and another elasto-plastic limestone layer (based on Carmichael, 1982; Pollard and Fletcher, 2005; Jaeger et al., 2007). The contacts between layers in the deforming block have been modelled as glued contacts. Other material properties used in this study are shown in Table 1. These inelastic material model permits permanent strains to develop in response to the applied oblique load. This model setup, with a frictional detachment and weak layers interbedded within the sequence, would resemble a common stratigraphic configuration found in various fold-and-thrust belts, such as the Dezful Embayment in the Zagros belt, Iran (e.g., Ruh et al., 2017; Derikvand et al., 2018; Sarkarinejad et al., 2018) or the eastern Jura belt (e.g., Malz et al., 2016; Nussbaum et al., 2017), as well as in some orogenic basins, such as the Malargüe group in the Neuquén basin, Argentina (Balgord and Carrapa, 2016).

Oblique convergence is modelled by imposing a given displacement (Fig. 2) to the active upper block. Block 1 is fixed in all directions (i.e., an encastre boundary condition), block 3 is the mobile backstop and block 2, bounded by the two dipping faults, represents an inclined transpressional zone (Fig. 2). A regional oblique shortening of 16% (3 km shortening) is imposed along the outer boundary of the mobile backstop

Table 1
Summary of material properties and parameters used in the inclined transpression zone model.

Layers	Parameter	Unit	Constant values
Layers 1 and 3: Limestone	Density, ρ	kg/m^3	2700
	Cohesion, C	MPa	15
	Young's modulus, E	GPa	48
	Poisson's ratio, ν	–	0.25
	Internal friction angle	°	40
	Tensile strength	MPa	12
	Compression strength	MPa	102
	Shear strength	MPa	25
	Porosity	%	5
Layer 2: Marl	Density, ρ	kg/m^3	2100
	Cohesion, C	MPa	2.5
	Young's modulus, E	GPa	0.2
	Poisson's ratio, ν	–	0.2
	Internal friction angle	°	30
	Tensile strength	MPa	0.2
	Compression strength	MPa	55
	Shear strength	MPa	0.7
	Porosity	%	10

under a convergence angle (angle α between the imposed convergence vector and the line perpendicular to the transpression zone boundary) of 25° (Fig. 2a, c), resulting in a pure shear-dominated transpression. Imposing displacements, instead of traction, allows formulating a model that is consistent with field observations and obviates the need to infer stresses (Fig. 2). The model width (along the X-axis) is constant during oblique convergence. Numerically, free surface boundary conditions are applied on the top model face, thus permitting self-consistent evolution of topography. In addition, both lateral boundary conditions are defined as free-slip along the boundary planes (Fig. 2c). Acceleration due to gravity (9.81 m/s^2) is imposed throughout the deformation as a body force. Due to the presence of the mechanical layering and inclined boundaries within the model blocks, we chose the recommended automatic time increment option in ABAQUS™. A choice of maximum and minimum allowable time increments of 0.01 for a total model time of 1.00 unit ensures that ABAQUS™ will choose a computationally efficient step size. This also ensures that the model output is written close to selected increments of interest (for example, every 0.1 units of time). The finite element mesh for the entire upper deforming block comprises 15,032 modified hexahedron elements having eight corner nodes. These elements are recommended for complex three-dimensional contact analysis in ABAQUS™. Mesh resolution was 1 km, which was determined by comparing results among multiple meshes created with different element size ranging from 600 m to 1.5 km and model geometries. The choice of element size was a compromise between output resolution and computational efficiency. According to the 3D nature of the study model, each interior node has three degrees of freedom. We utilized reduced-integration hexahedral plane strain elements that conform to the predefined surface-to-surface contacts and reduced stress artefacts arise from frictional slip.

We use the 3D FE-modelling to simulate stress and strain features recorded in the transpression zone. Due to the continuum nature of the FE-analysis, the model presented here cannot simulate the brittle failure of rocks, characteristic of shallow crustal levels. However, by using the orientation of the principal stresses and strains that develop in the modelled transpression zone, it is possible to show and predict the most probable orientation of brittle structures that could develop during deformation.

3. Results

In this Lagrangian model, the meshes are deformed reproducing crustal blocks and material deformation. Oblique convergence, pre-existing inclined faults, mechanical stratigraphy and the nature of the

frictional detachment horizons (lower frictional detachment at the base and intermediate viscous detachment at the marl layer) play significant roles in the structural evolution, strain localisation, importance of brittle and ductile structures, and spatial distribution of deformation along and across the inclined transpression zone. Under oblique convergence, ductile deformation localises preferentially within the transpression zone bounded by the two dipping faults and in block 3. Upon imposing the total oblique convergence in an incremental manner, the model block evolves under a combination of slip (discrete deformation) on the faults and distributed deformation within the 'active' blocks. The 'active' blocks overall undergo oblique contraction, which results in shortening, and thickening in the horizontal and vertical directions, respectively. It is important to note that uplift and subsidence develop in our models only as a result of the amount of oblique convergence, and other processes such as sedimentation, and isostatic response have not been considered. This is a simplification, as these processes are known to affect uplift and subsidence. We expect, however, that the general pattern of surface deformation is accurate.

3.1. Geometry, kinematics and mechanics of the modelled inclined transpression zone

The FE-model results presented in this study are orientation and magnitude of plastic strain, shear strain, displacement, and stress (Figs. 3–8). We use this information to predict the most probable location, orientation and behaviour of real structures (folds and faults) that would develop during deformation.

Deformation throughout the experiment affects the three active blocks albeit differently (Fig. 3). A wedge-shaped deformed volume (positive flower-shaped structure) formed at the central part of the model, completely affecting block 2, and whose limits are located at blocks 1 and 3. The mobile backstop (block 3) was deformed more intensively than the fixed one (block 1), and plasticity developed over a total distance of about 12 km within active blocks (Fig. 6). This wedge-shaped zone entirely accommodated the transpressional deformation imposed by the oblique convergence boundary conditions, via slip on arrays of faults and the development of systematic minor fold sets as penetrative strain (cf., Burberry, 2015). Layers in the mobile backstop were tilted and flexed upward above fault 2. An inclined, tabular-shaped transpressional zone formed in block 2 bounded by the two parallel pre-existing faults (faults 1 and 2) (Figs. 3 and 6d).

Oblique convergence at the model was accommodated by discrete deformation (simple shearing/slip) at the two main pre-existing faults and by distributed brittle and ductile deformation at active blocks, localised preferentially at the tabular-shaped transpression zone. Maximum incremental strains were concentrated at this transpressional zone and particularly at its boundaries, although fault 2 presents higher strain values (=1.3–2.6) than fault 1 (=0.8–1.3).

Stress and strain orientations and magnitudes during the experiment suggest that oblique contraction at the active blocks resulted mainly in layer-parallel shortening (parallel to the Y-axis), compensated by lengthening in the horizontal (X-axis parallel) and vertical directions, respectively accommodated via layer-parallel extension and up-dip extrusion mainly produced at the frontal part of the two main oblique faults (Figs. 3 and 6). This heterogeneous thickening results from increased normal stress across the inclined fault boundaries at depth (Fig. 4), which causes distributed deformation. At the end of the experiment, after 3 km of backstop oblique convergence, 16% of orthogonal shortening was compensated by 40% of vertical extrusion (the total thickness increased from 9.5 to 13.2 km). Shortening at the tabular transpression zone and lateral extrusion (~28%) should have compensated the rest of oblique convergence, and/or volume loss with penetrative strain took place. Overall, the wedge-shaped zone was deformed by plunging oblique folds, oblique-slip faults, thrust stacks and distributed distortion within the inclined transpression zone (Figs. 3–6). The main structures are described in detail in the following paragraphs.

According to the strain distribution, we can identify three fault types in the wedge-shaped zone (Figs. 3 and 6d): (i) the main dipping thrusts (i.e., forethrusts or pro-shears in Leever et al., 2011), localised here at the pre-existing inclined faults and also at the fixed block; (ii) oblique shear bands at the tabular zone that cross-cut bedding planes; and (iii) backthrust planes (pro-wedge thrust faults or retro-shears in Leever et al., 2011) that develop within the mobile backstop due to a local contractional bend (the type-I backthrust model in Xu et al., 2015), and also the transpression zone. Pro-shears in the fixed block have smaller dip angles (~20–35°) than backthrusts (~40–50°) and the main oblique shears (~65°) (Fig. 3). In general, fore- and backthrusts were more penetrative in competent layers (limestone layers) than in the incompetent layer (marl). Slip on the fault planes is oblique and faults exhibit dip refraction as a function of the lithology. In the limestone (more brittle) and marl (less brittle) layers, faults dip 65–80° and 40–55°, respectively (Fig. 4). A forethrust or footwall shortcut thrust (Fig. 3) is a characteristic feature of basins under tectonic shortening. This leads to

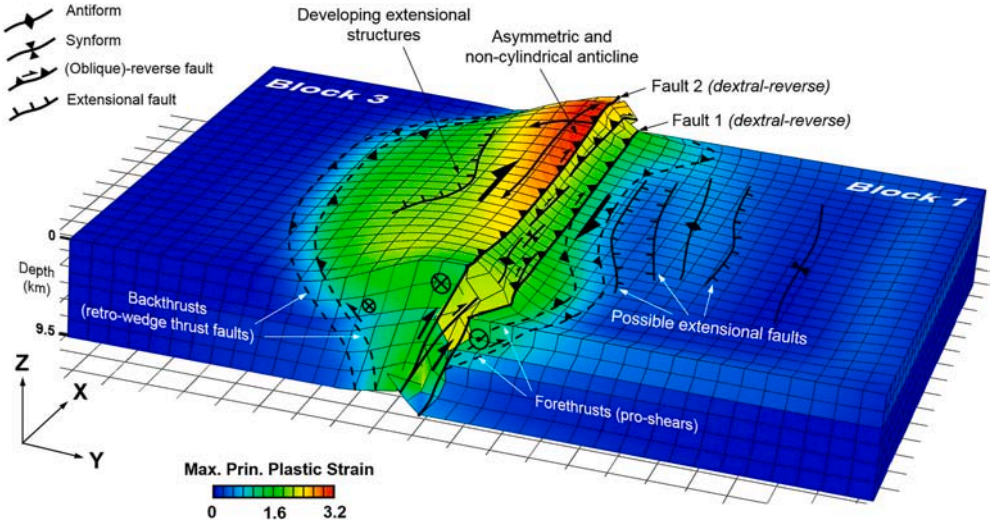

Fig. 3. Observed structural geometry, internal deformation and distribution of maximum principal plastic strain resulting from oblique convergence for a heterogeneous and anisotropic mechanical model of the inclined, brittle-ductile transpression zone. The strain values for all elements are obtained by integrating the strain rate numerically in a material frame and the maximum plastic strain is the largest positive contractional strains.

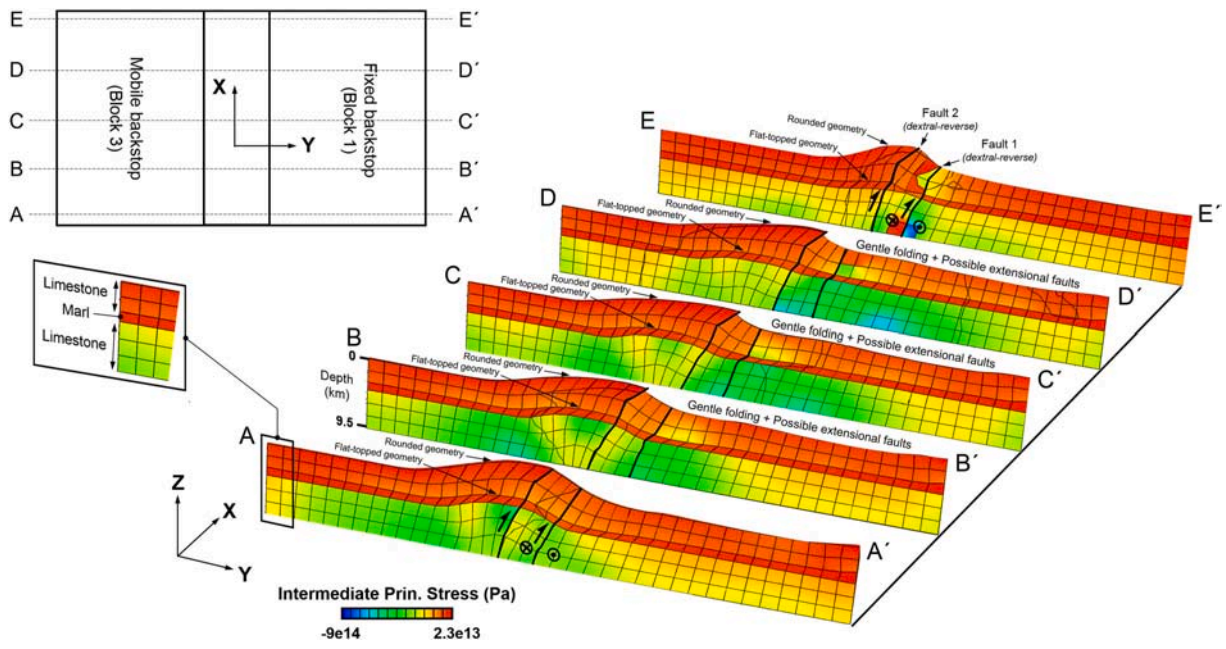

Fig. 4. Vertical cross-sections of the model with distribution of the intermediate principal stress (same colour scale for all profiles). The locations of the vertical sections are shown in the left map view. The model actually underwent a contraction and the minus sign in the stress bar scale indicates minimum values of compressive stress and auto limit calculations. When the initial conditions is considered (zero stress and strain) the recovery in elastic rheology will appear as a negative value. (For interpretation of the references to colour in this figure legend, the reader is referred to the Web version of this article.)

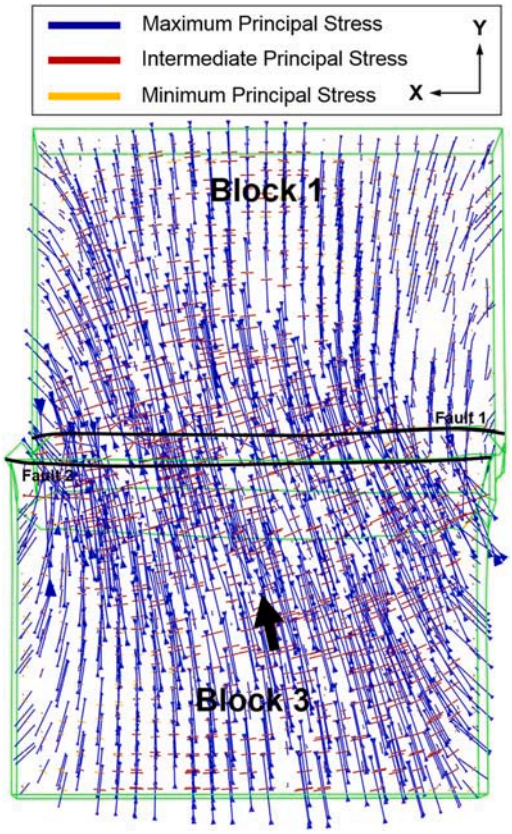

Fig. 5. Top view of FE-model results representing the spatial distribution of principal stress axes (also compare with Fig. 9b in Authemayou et al., 2006).

the footwall shortcut thrust faults to break off from the original high angle to a lower angle towards the surface (Powell, 1987; McClay and Buchanan, 1992).

Regarding the tabular, inclined transpressional zone of block 2, horizontal and vertical displacement of material caused the oblique (dextral-reverse) simple shearing along the bounding faults (faults 1 and 2), as seen by the asymmetric distribution of shear stress/strain (Fig. 7a). These two faults accumulate large amounts of strain (higher value of incremental shear strain), although fault 2 accommodates higher shear strain values, and it is considered more active, than fault 1. Secondary, conjugate fault zones also accommodate oblique slip and contribute to uplift. Much smaller strains are accumulated at the backthrust, which propagates upwards from the basal detachment, and the shear bands (cross-cutting bedding planes) of the wedge.

Dextral-reverse slip on faults 1 and 2 creates offset between the model blocks. It also causes the displacement vectors (or particle paths in the XY horizontal plane) within this transpressional zone to rotate counter-clockwise with respect to vectors in the undeformed sector, forming a ca. 20–30° angle with the backstops (Fig. 8b). The final top view architecture of the model reveals that this oblique fault system deviates from the linear trend reproduced in orthogonal experiments (e.g., Marques and Nogueira, 2008; Graveleau et al., 2012 and references therein) and attains a somewhat curved trend. Overall, a variety of damage zones, particularly interaction, wall, and distributed damage zones (see Peacock et al., 2017 for details on damage zones) are developed as a result of oblique convergence throughout the transpression zone.

Fold hinges plunge and are not straight, so that folding and thickening of the mobile backstop (block 3) produced a non-cylindrical, asymmetric, bi-vergent anticline (hangingwall anticline or pop-up structure), which is flanked by oblique thrusts with permanent strains developed principally in the steep forelimb (or retro-wedge) (Figs. 3 and 4). This pop-up structure was bounded by an oblique backthrust at block 3 and one of the pre-existing oblique faults (fault 2) (Fig. 6). The shear strain is high in the front of this asymmetric anticline (close to fault 2) and progressively decreases toward the trailing parts of the mobile backstop. This strain asymmetry is the result of the basal boundary condition and the tip line of the pre-existing inclined fault, and likely produced an 850 m-high scarp at the front of this anticline.

Deformation also causes tilting at the inclined fault 2 edge and

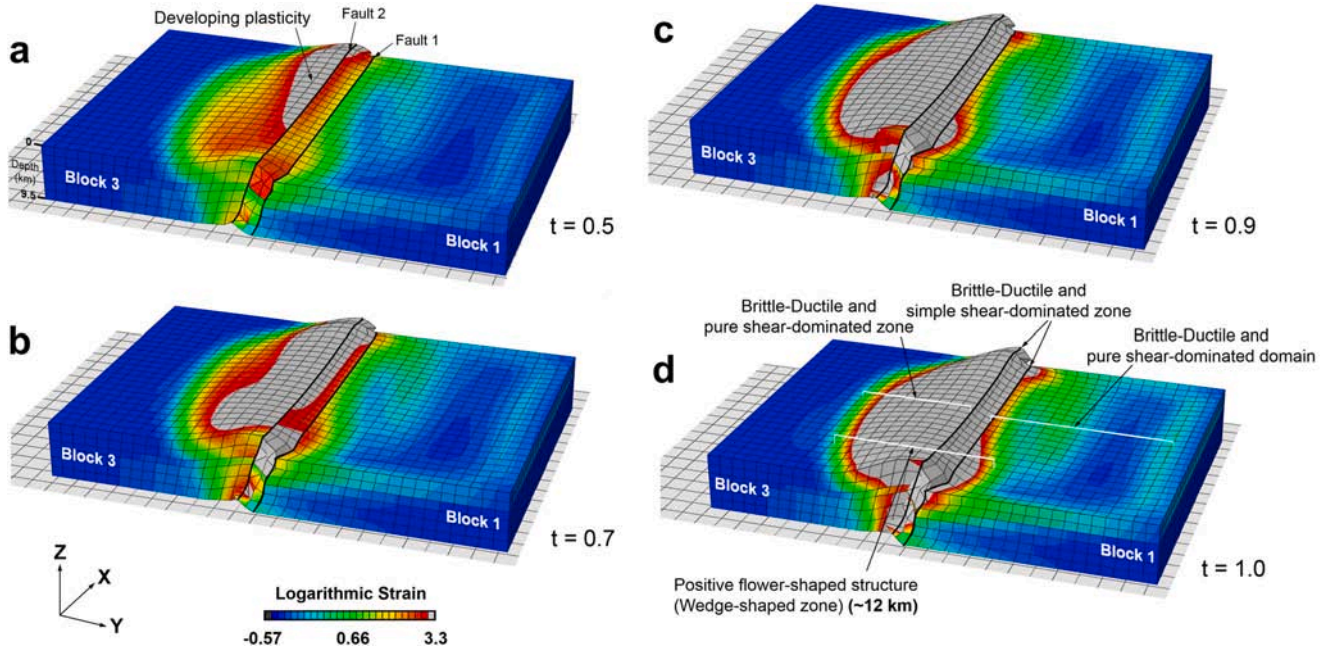

Fig. 6. Surface topography and interpretation of the magnitude and distribution of progressive deformation in the FE-model at different time steps a) 0.5, b) 0.7, c) 0.9, and d) 1.0 intervals of ca. 8%, 11%, 12%, and 16%, respectively (same strain bar scale for all models). Since nonlinear geometric effects are active, an efficient measure of strain is the logarithmic strain. The imposed plastic behaviour implies that in order to suffer permanent deformation the material must attain its passed yielding point (which is evaluated by comparing maximum Von Mises stress and yield stress at each element).

steepening of the anticline backlimb due to limb rotation with hinge migration, a common feature in transpressional folding (Tikoff and Peterson, 1998; Titus et al., 2007). Frehner (2016) showed that the fold hinges are not passive material lines, but active markers that migrate during transpression. This anticline would have been favored by the frictional surface between the active blocks and the basic rigid block, and the presence of an inclined fault plane (fault 2). The fold would contribute to the tectonic thickening of the hangingwall (cf. Koyi and Maillot, 2007). The anticline is linked with a syncline towards the rear of the displacement block 3, and the whole structure could be considered as a 'concave fault bend fold' (Brandes and Tanner, 2014; Ziesch et al., 2014). However, unlike the fault-parallel flow model due to pure contraction (Ziesch et al., 2014), here, the flow path is oblique to the inclined fault. In this regard, different structural styles occur at the active blocks, such as pressure solution cleavages, backthrusts and extensional fractures depending on stress boundary conditions and mechanical stratigraphy. Moreover, cross-sections across the study model (Fig. 4) show that the mechanical stratigraphy influences folding geometries, so that more brittle layers (limestone layers) lead to more rounded fold geometry whereas less brittle layer (marl layer) lead to sharp-hinged and flat-topped fold geometry. Also, the lower limestone layer shows wider hinge zones than the upper limestone layer due to increases in thickness and depth (Fig. 4).

As oblique convergence increases, inclined transpression is accommodated by progressively greater slip at the pre-existing faults while the anticline in the mobile backstop grows by increasing its amplitude rather than its width. Furthermore, the tabular-shaped transpression zone progressively rotates cause the anticline to rotate progressively from upright to overturned. This rotation is accompanied by stretching and thinning of the forelimb, which can causing local strain partitioning (e.g., Carreras and Druguet, 2019). Therefore, this deformation generates local asymmetric synclines verging toward the fixed backstop (Figs. 3 and 4).

Compressive stress developed in the tabular-shaped transpressional zone and the non-cylindrical, asymmetric anticline, where the three principal stress axes are oblique with respect to the pre-existing faults (transpression zone boundaries) (Fig. 5). The principal axes of the stress tensor rotate in these zones (Fig. 5), such that the value of the horizontal stress decreases enough for tension to occur close to the outer arc of the uplifted areas.

3.2. Variation of slip along inclined fault segments

According to high maximum values of shear (=5.57e^7 Pa) and normal (=4.39e^8 Pa) stresses on sliding surfaces (Fig. 7a and b), slip can occur along fault 2, although relatively low friction coefficient (<0.2) is required. Moreover, the slip tendency (i.e., the ratio of resolved shear and normal stresses acting on the fault surface, Morris et al., 1996) is relatively low (=0.13). This low value is due to the existence of the high angle ramp and the stress localisation at the fault interface, such that the fault acts as a mechanical heterogeneity. Moreover, the upper limestone layer shows a higher value of the intermediate normal stress than the lower limestone layer (Fig. 4), which may be related to the incompetent marl layer between them and the thickness of the lower limestone layer. In general, steep fault segments (dip angle > 60°) through competent units such as limestone, have lower slip tendency than gentler fault segments (dip angle < 60°) because of the lower resolved shear stress acting on those steep surface segments (see Ferrill et al., 2017; Rosas et al., 2017 for details). Introducing elasto-plastic rheology results in markedly different and asymmetric slip distribution along the inclined fault surfaces, with more slip reaching the sub-surface and greater localisation (Fig. 7c and d). On the other hand, model results indicate shallow faulting is also associated with mechanical layering and plastic yielding. Given that new faults form during progressive oblique convergence, the main oblique-reverse faults (i.e., transpression zone boundaries) with higher slip tendencies are represented by multiple and asymmetric displacement values from high to low. Morris et al. (2016), in line with this subject, proposed a conceptual form of the nonlinear relationship between slip tendency and the observed fault displacement (Fig. 7 in Morris et al., 2016). It should be noted that the regions for higher slip tendency overlap with areas of volume loss or dilation tendency, suggesting that faults/fractures could be developed as a mixed-mode failure type (e.g., Stephens et al., 2017).

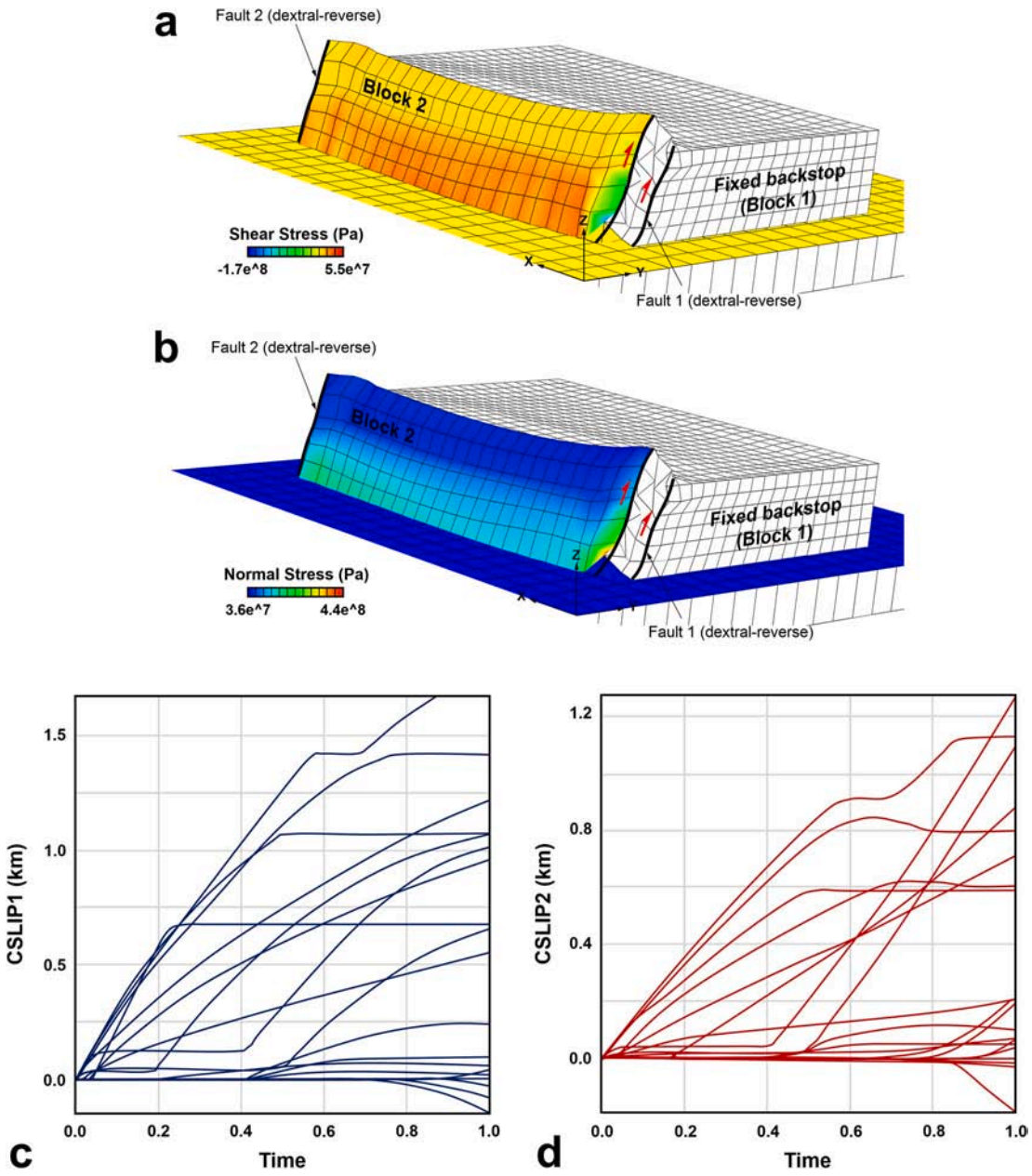

Fig. 7. Modelling results of distribution of a) shear stress; and b) normal stress along fault 2. c, d) Variations in slip magnitude versus time (increasing oblique convergence). In 3D FE-models, there are two orthogonal slip directions along- and across-strike of fault 2 (CSLIP1 and CSLIP2 in ABAQUS™) for each point at a given contact surface, which together with the surface normal form an orthogonal coordinate system at every point on the surface, and therefore higher slip values resulted in higher nodal displacement. Negative magnitudes of CSLIP indicate that the node has moved in the negative slip direction.

3.3. Spatial variation of the displacement vectors across the model

Model results show that the resultant displacement leads to the final surface topography after shortening by 16%. As the model block (crust) is converged above the inclined boundary, it bulges and forms the inclined transpression (or orogenic belt in crustal-scale) of elevated topography. Indeed, we present here a displacement map for the study model. During model oblique convergence, displacement vectors (Fig. 8b and c) show: *(i)* The X component gradually vanishes away from the applied far-field stress, with a clear step at the oblique-reverse fault 1; *(ii)* The Z component increases from the bottom to the top, and gradually vanishes away from hagingwall-anticline; *(iii)* In the hangingwall blocks, displacement vectors rotated from horizontal near applied stress's boundary toward higher dip angles till they become slightly oblique to sub-parallel to the transpression zone boundaries (Fig. 8b). In the footwall block, the X component decreases and displacement vectors show an almost pure Y component; *(iv)* Shortening was accommodated by layer thickening and displacement along both oblique-reverse faults; *(v)* The map integrating displacement show the curvilinear (non-linear) pattern in the hangingwall block and transpression zone (Fig. 8b), with trajectories dipping around 20–30° in hangingwall block, and 35–50° in the transpression zone, thus oblique to the transpression zone boundaries (Fig. 8c). Furthermore, displacement vectors at the base of the hangingwall block and the transpression zone dips <5°, and are thus sub-horizontal (Fig. 8c) (e.g., analogue model with the 70° dipping indenter in Cruz et al., 2008); *(vi)* Displacement in the footwall blocks immediately below the transpression zone boundary was parallel to the Y axis and sub-horizontal (Fig. 8b and c); *(vii)* On the left side of the inclined transpression zone (map view) (Fig. 8b), the displacement vectors have an increasing component of lateral

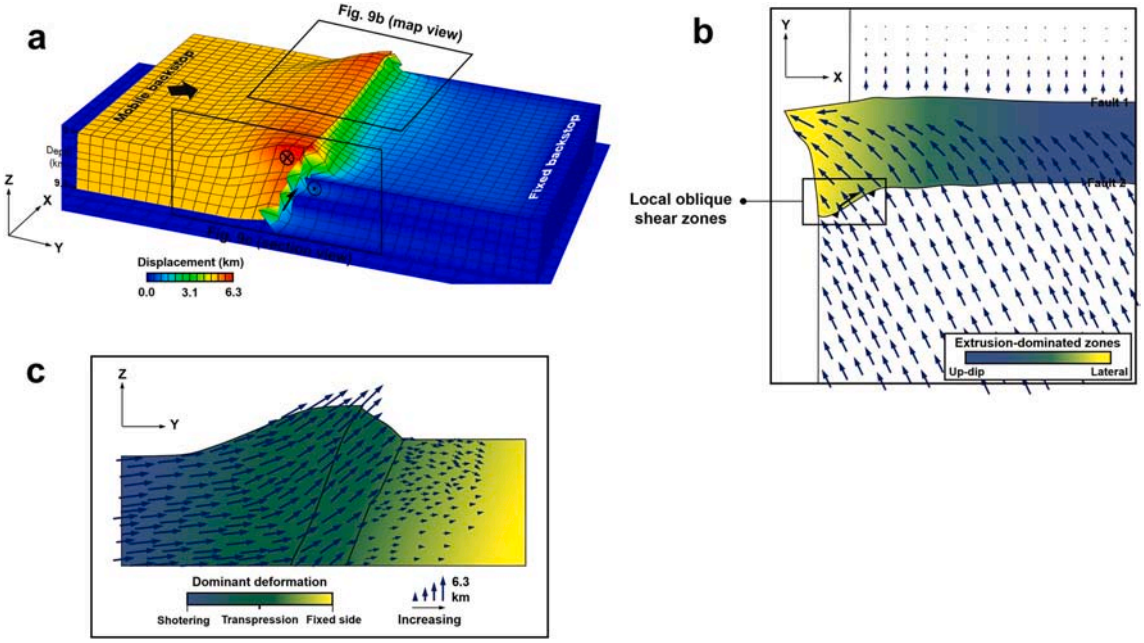

Fig. 8. a) Modelling result for displacement distribution. b) Top-view interpretation of displacement vectors within selected part of Fig. 7a, according to the colour spectrum, the transition from the central part of the transpression zone to its lateral part is characterized by a gradual transition of strain regime giving place to lateral extrusion. c) Section view interpretation of displacement vectors within selected part in Fig. 7a. According to the colour spectrum, the displacement vectors gradually deviate from the outer parts of the mobile block (block 3, left part of the section) to the transpression zone, so that angle between the displacement vectors gradually increases with respect to the Y-axis. (For interpretation of the references to colour in this figure legend, the reader is referred to the Web version of this article.)

displacement in the direction of the weak lateral component, i.e., vectors deviate from the convergence direction and rotate towards the weak lateral component as lateral extrusion; *(viii)* The displacement partitions into various amounts of up-dip extrusion (as non-cylindrical fold) and heterogeneous strain throughout the transpressional system.

4. Discussion

4.1. Deformation of the model

The purpose of the mechanical models in this study is not to simulate the exact geometry of the deformation structures documented in specific natural examples but to contribute to a general understanding of the basic mechanical processes and the kinematic regime that might have influenced their development. The numerical results present a strain partitioning pattern characterized by two main domains, each of which accommodated different components of transpressive deformation. Narrow domains at the two pre-existing faults accommodated simple shear-dominated dextral transpression whereas a wide domain deformed by pure shear-dominated triclinic transpression.

In the wide, pure shear-dominated domain, the displacement was partitioned between mainly dextral and dextral-reverse faults sub-parallel with the main boundaries, and reverse faults and associated folds obliquely oriented (0–30°) to them (i.e., axial length of fold is oblique to the boundaries and the fixed backstop). This agrees with results from other kinematic and analogue models (e.g., Casas et al., 2001; Leever et al., 2011; Díaz-Azpiroz et al., 2014; Barcos et al., 2015; Calignano et al., 2017). The trend of the transpression zone is parallel with the backstops and shortening and related oblique lateral extrusion (25–40° with respect to the main inclined transpression zone boundaries) is produced by oblique-reverse faults and folds. Folds show no evidence of rotation in either model. This seems to differ from other cases of folding in monoclinic transpression zones simulated by analytical (e.g., Tikoff and Teyssier, 1994; Titus et al., 2007), analogue (Tikoff and Peterson, 1998; Ghosh et al., 2014), and numerical modelling (Frehner, 2016; Nabavi et al., 2018a) in which folds rotate or accommodate to finite strain axes re-orientation during progressive deformation. Fold axes in the FE-model follow a curved path and takes place mainly by hinge-parallel extension and elongated markers. Stretching parallel with the X-axis is accommodated by the principal strike-slip faults. Transpression zone-parallel stretch and oblique shortening, both resulting from the coaxial flow component, would lead to space problem and strain incompatibility (e.g., Vitale and Mazzoli, 2008), unless they are accommodated by lateral and/or up-dip extrusion (e.g., Fernández and Díaz-Azpiroz, 2009; Sarkarinejad et al., 2009; Mukherjee and Koyi, 2010; Viola and Henderson, 2010; Mukherjee et al., 2012), which is the case of the study model.

Lateral extrusion entails the combined effects of material (or tectonic) escape and gravitational collapse of a weak wedge in response to oblique convergence under conditions of inclined and lateral boundaries so that extrusion is oriented at a high angle to the convergence direction (Fig. 8b) (e.g., Ratschbacher et al., 1991; van Gelder et al., 2017). The highest degree of lateral extrusion occurs near the fixed backstop boundary (fault 2, Fig. 8b). Following such lateral extrusion, some local oblique-reverse faults and shear zones develop in that area, spatially related to vertical to overturned fold limbs, so that their orientation and vergence are similar (Fig. 8b, d). In this regard, important parameters influencing the extrusion (amount and orientation) and the resulting deformation patterns are the dip of boundaries, the angle of oblique convergence, the mechanical stratigraphy, the amount of convergence and the width of the contracted zones.

Additionally, deformation in the brittle layers is mainly accommodated by thrust faults, which are spatially related to thickening in the underlying ductile layer, suggesting high mechanical coupling. Furthermore, the results show that low shear strain and shear stress are necessary for backthrusts and shear bands to form (e.g., Ruh et al., 2012, 2014). Using critical taper theory it has been shown that backthrusts preferentially form at low taper angles. For medium obliquities ($\alpha \leq$ 45–55°), thrust faults dips are steeper and their number is lower in oblique convergence than in purely frontal convergence deformation

styles (e.g., Richard and Cobbold, 1990; McClay et al., 2004; Graveleau et al., 2012; Xu et al., 2015; Bose and Mukherjee, 2019).

4.2. Strain partitioning in transpression

Discrete strain partitioning between narrow, strike-slip dominated domains and wider, contraction dominated domains, is a common feature in oblique convergent systems (e.g., Jones and Tanner, 1995; Bowman et al., 2003). Strain partitioning of the oblique convergence involve complex systems of geologic structures. Therefore, it causes spatial and temporal redistribution of stress and strain fields over and along the part of the deforming plate and or pre-existing faults. Several previous works suggest that such strain partitioning take place once a major strike-slip fault is formed, which only occurs after a minimum of strain is accumulated (e.g., Braun and Beaumont, 1995; Burbidge and Braun, 1998; McClay et al., 2004; Leever et al., 2011). It is noteworthy that these analogue and numerical models normally generate a transpressional wedge above a velocity discontinuity at the bottom of the model. This would correspond to natural oblique convergence acting on layered sequences with no previous structures. In these situations, the strike-slip fault that triggers strain partitioning forms during strain accumulation. However, reactivation of inherited structures is a very common situation in nature (e.g., Holdsworth et al., 2001; Tavarnelli et al., 2004). In this model, this is simulated by two pre-existing faults (faults 1 and 2). The activity of slip along these major rheological steep planar boundaries favors the early nucleation of boundary-parallel deformation zones where simple shear concentrates. Consequently, strike-slip dominated, narrow transpressional zones nucleate related to these faults at the very onset of deformation. Therefore, strain partitioning is active from early deformation stages, even in low oblique, contractional dominated systems (e.g., Barcos et al., 2016).

Observations from this and previous models allow us to discuss how the main characteristics of the nucleating structure control the shape of the resulting transpressional zone. Transpressional wedges formed spontaneously above a basement fault typically present slightly asymmetric, doubly-verging geometries with a main strike-slip fault in the center (e.g., Braun and Beaumont, 1995; Burbidge and Braun, 1998; Casas et al., 2001; Leever et al., 2011). By contrast, when inherited, parallel, strongly dipping faults nucleate deformation, tabular transpressional zones are formed between them. In these cases, the rheology of the deforming medium is relevant. If the bounding blocks related by the two parallel faults show significant rheological differences with the tabular zone, narrow, strike-slip dominated zones form at these boundaries (e.g., the Torcal shear zone, Díaz-Azpiroz et al., 2014; Barcos et al., 2016). In our model there is no such rheological difference, thus the blocks bounded by the inherited faults do not act as rigid backstops. This permits progressive deformation to propagate outwards from the seminal tabular zone generating a transpressional wedge (Fig. 6). However, in this case, the wedge is strongly asymmetric, with very little deformation affecting the block located ahead the tabular zone (block 1) (Figs. 3, 4 and 6). It shows a single, narrow, strike-slip dominated zone located at the boundary with a semi-rigid domain, and a wide wedge with distributed, contraction dominated deformation, whose structures verge away from the strike-slip dominated zone (Figs. 3, 4 and 6). Deformation within this domain is homogeneously distributed at early deformation stages and becomes more evident with the later appearance of predominantly shortening structures (Fig. 6). These results illustrate strain partitioning in pure shear-dominated transpression is strong. However, with increasing heterogeneity of the deforming sequence, strain partitioning are expected to deviate from kinematic predictions (Jiang and Bentley, 2012; Carreras et al., 2013). Furthermore, increasing convergence, which is associated with a nonlinear increase of shear strain along the model length, can lead to thrust nappes and fold nappes (e.g., Alsop et al., 2010; von Tscharner et al., 2016; Nabavi et al., 2017b). A similar structural pattern is observed in northwestern part of the Zagros belt, Iran (e.g., Authemayou et al., 2006), where the dextral Main Recent Fault (MRF) splits in two subparallel, strongly dipping planes defining a parallel zone, would correspond to our faults 1 and 2 and the tabular zone in between; the Simply Folded Belt (or foreland fold-and-thrust belt, SW verging, towards the displacement) would be represented by our block 1 and the zone to the NE of the MRF (or hinterland fold-and-thrust belt) would be a domain with large deformation akin to our block 3. The main difference is the dipping direction of the master faults (forwards in our FE-model, backwards in the Zagros). Although all these faults dip steeply and thus they would likely produce minor differences in the final result.

However, the structures developed in natural examples (e.g., Barcos et al., 2011, 2015; Díaz-Azpiroz et al., 2014; Barcos, 2015; Nabavi et al., 2017b; Alonso-Henar et al., 2020), analogue models (e.g., Casas et al., 2001; Leever et al., 2011; Barcos et al., 2016; Crespo-Blanc et al., 2018; Fedorik et al., 2019), and the presented FE-model of inclined transpression zones, such as positive flower-like structures, brittle-ductile shear zones that generate meso-scale S–C-like structures, inclined strain fabrics (tectonic foliation and tectonic lineation), non-cylindrical folds, normal fault zones, and oblique-reverse faults, show an overall heterogeneity distributed within the area. Hence, we understand that strain partitioning develop during the evolution process of deformation under oblique convergence.

Strain paths and deformation styles have been suggested to follow non-linear paths in transpression and transtension (Fossen et al., 2019), which can be enhanced by the presence of mechanical heterogeneties. These heterogeneities are simulated in our FE-model by the presence of mechanical stratigraphy, and two inclined faults that correspond to two planar velocity discontinuities of the model set-up. The block 1 is represented in many analytical and analogue models (fixed backstop). These boundary conditions are interpreted as pre-existing planar steep structures that play a main role in both the localisation of the transpression zone and its strong strain partitioning (Tavarnelli et al., 2004; Barcos et al., 2016). In general, the bulk mechanical strength of a layered model plays a prominent role in influencing the overall strain localisation. In this study, the model made up of an incompetent layer between two competent layers, hence, the refraction of the strains across the layer interface increases with increasing competence contrast and suggests that different sets of linking faults could develop at different structural depths (Fig. 6) (e.g., Druguet et al., 2009). The activity of slip along these major rheological steep planar boundaries favours the early nucleation of boundary-parallel deformation zones where simple shear concentrates. For high values of obliquity (convergence angles of 4–30° based on Leever et al., 2011), the long-term kinematic evolution of transpression zones can be divided into three distinct stages: indeed, an initial ‘distributed strain’ stage, then an ‘oblique wedge’ stage, and finally a ‘strain partitioning’ stage. An interesting result, regarding possible comparison with analytical and analogue models, is that although there is no such a rigid backstop in the model and many researches consider the fixed backstop to be completely rigid, deformation in block 1 (more often by gentle folding; and may be with some possible extensional faults, so that extensional faulting can be associated with oblique convergence; see Casini et al., 2018 for examples in the Zagros belt, Iran) (Figs. 3 and 4) is significantly lower than in the other two, so a semi-rigid behaviour could be considered.

4.3. Kinematics and extrusion of the transpressive zone

According to the orientation of particle paths (20–30°) with respect to the transpression zone boundaries, the kinematic vorticity number (W_k) of the entire model can be estimated to be 0.4–0.65 (Fig. 9a). Furthermore, according to the displacement partitioning (Fig. 8), it can be hypothesized that the angle between the extrusion direction and the dip of the transpression zone (angle ν in Fernández and Díaz-Azpiroz, 2009) locally deviates from 0° ($\nu \neq 0°$) along the dextral-reverse fault boundary. In this sense, variations in the amount of vertical extrusion from point to point along the transpression zone suggest that ν can reach

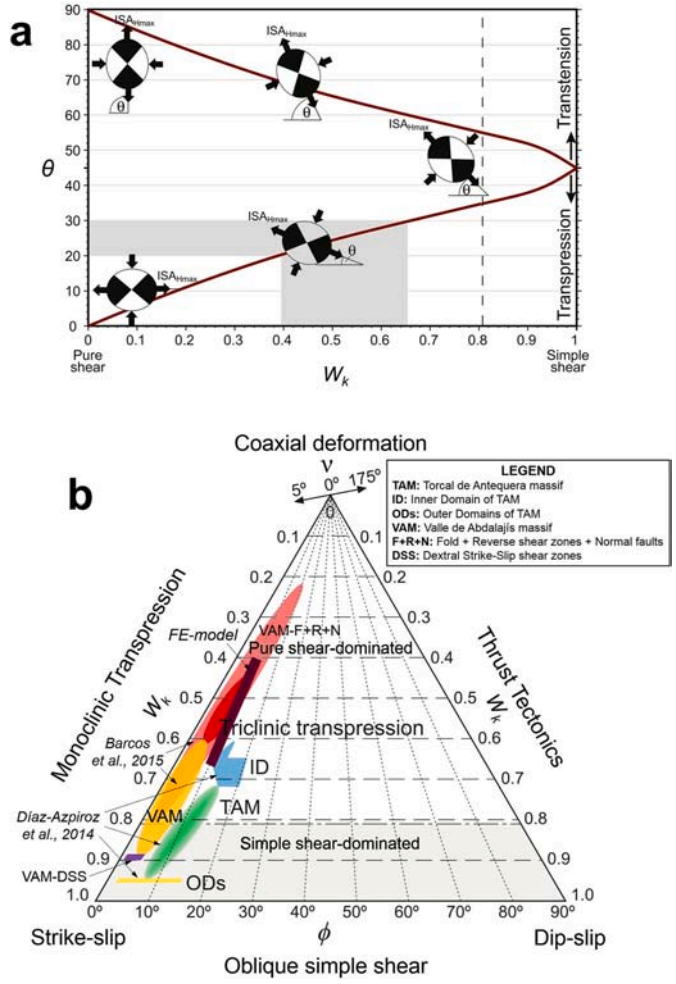

Fig. 9. a) Relationship between θ (angle of convergence of Fossen et al., 2013; which equal the value of angle α considered in this work) and W_k (kinematic vorticity number) (after Fossen et al., 2013). b) Strain partitioning within the study finite element model as viewed in a strain triangle proposed by Díaz-Azpiroz et al. (2014) inspired in that Jones et al. (2004), where FE-modelling results (dark purple line) compared with the kinematic transpression parameters for bulk strain within the Torcal de Antequera massif (Díaz-Azpiroz et al., 2014), and the Valle de Abdalajís massif (Barcos et al., 2015). (For interpretation of the references to colour in this figure legend, the reader is referred to the Web version of this article.)

up to ~18°. In addition, the angle between oblique simple shearing direction and the strike of the transpression zone (φ in Lin et al., 1998) is ~10° (Fig. 9b). Hence, the angle between the simple shearing and the extrusion directions (angle ζ of Fernández and Díaz-Azpiroz, 2009) is below 90° (~82°). The shape of the strain ellipsoid in transpressional deformation strongly depends on W_k and angle ζ (Fernández and Díaz-Azpiroz, 2009). Accordingly, the values of these two parameters deduced from our results (ζ > 40° and W_k = 0.4–0.65) would theoretically produce, strain ellipsoids that clearly deviate from the plane-strain line, and plot in well within the flattening field of the Flinn diagram. In addition, non-parallelism between displacement vectors and the faults limiting the blocks (Fig. 8b and c), evidencing shortening and lengthening along the Y- and X-axis, respectively, also suggests that flattening took place in the deforming blocks. Therefore, the results of the FE-model plot on the triclinic transpression area (pure-shear dominated domain) of the strain triangle (Fig. 9b).

The relative obliquity of the simple shear component creates amplification (corresponding to the fold growth in the vertical or Z-direction; Frehner, 2014, 2016) and elongation (correspond to the fold growth in X-direction or parallel to fold axis; Frehner, 2014, 2016) of non-cylindrical antiforms and the system of obliquely plunging lineations. A similar inclined extrusion is also observed along the transpression zone in the Barcos et al. (2016) analogue model, and in the form of parabolic and bell-shaped velocity profile, respectively, in Newtonian and non-Newtonian materials (e.g., Mukherjee and Koyi, 2010; Mukherjee et al., 2012; Mukherjee, 2013). These findings show that the transpression zone has an important role on extrusion kinematics and velocity (e.g., Marques et al., 2018a, 2018b).

According to the FE-modelling results (Fig. 3), deformation is distributed upward toward the Earth's surface and across a zone that is kilometres wide, progressively narrowing with depth. In general, FE-modelling results show that the contraction deformation is widely distributed developing brittle and ductile structures and due to the flow of the underlying plastic layer, therefore, the model can be considered as a case of 'distributed transpression' (Schreurs and Colletta, 1998, 2002; Sançar et al., 2015). Distributed deformation in oblique tectonic settings has been described in many studies over wide and complex zones ranging in scale from several hundred kilometres to several meters, with complex displacements, strain patterns, and rotational deformation (Molnar and Tapponier, 1975; McKenzie and Jackson, 1986; England, 1989; Schreurs and Colletta, 1998, 2002; Schreurs, 2003; Sançar et al., 2015). The results of our FE-model suggest that high-angle oblique-reverse faults can suffer a significant slip component, in addition to the amount of oblique convergence, if they are weak enough, which is related to the angle and coefficient of sliding friction, and fluid pressure. In experimental models, it can be done by the presence of a thin film of silicone putty along the pre-existing faults (e.g., Marques and Nogueira, 2008).

5. Conclusions

Combination of mechanical, geometrical, analytical and analogue models can provide a more accurate representation of inclined transpression zones and clarify some topics of this important issue. Natural examples of oblique convergence setting in transpression zones are inherently 3D and show inclined boundaries; hence, the evolution of inclined transpression zones is studied using 3D inelastic numerical finite-element modelling by applying a general triclinic inclined transpression model. In addition, use of inelastic constitutive relationships allows permanent strains to develop in response to the applied loads.

1) FE-modelling results demonstrate oblique convergence at the model was accommodated by discrete deformation at the main pre-existing inclined faults and by distributed brittle-ductile deformation at active blocks.
2) Oblique contraction at the active blocks resulted mainly in layer-parallel shortening, orthogonal to model outer boundaries, and lengthening in the horizontal and vertical directions, respectively accommodated via layer-parallel extension and up-dip extrusion. Lateral extrusion should have compensated the rest and/or volume loss took place.
3) Folding and thickening of the mobile backstop produced a non-cylindrical, asymmetric, bi-vergent anticline with permanent strains developed principally in the steep forelimb. Secondary, conjugate fault zones also accommodate oblique slip and contribute to uplift.
4) Displacement vectors (or particle paths in the XY horizontal plane) within transpressional zone are rotated counter-clockwise (ca. 20°–30°) with respect to vectors in the fixed sector. Areas with higher rotation values seem to correlate with those showing higher ellipticity values of the finite strain ellipsoids.
5) Inherited structures localise strike-slip motion, thus triggering strain partitioning from early deformation stages. A tabular transpression zone forms between pre-existing faults, while deformation propagates mainly towards the mobile block. The resulting transpression

wedge can be compared to some strongly asymmetric wedges nucleated at major faults under oblique convergence conditions.

6) In general, factor like the width of the transpressional zone, the dip of boundaries, the angle of oblique convergence, mechanical stratigraphy, amount of oblique convergence, and the presence of tectonic inheritance play important roles in strain localisation, the amount of localisation along the transpression zone (decreasing with increasing obliquity), and control along- and across-strike variation in the oblique convergence settings. Even if deformation is localised along a mobile backstop and the transpression zone, parts of the study model remain undeformed at the external areas, particularly at the fixed backstop.

Declaration of competing interest

The authors declare that they have no known competing financial interests or personal relationships that could have appeared to influence the work reported in this paper.

CRediT authorship contribution statement

Seyed Tohid Nabavi: Project administration, Conceptualization, Methodology, Software, Validation, Investigation, Visualization, Resources, Data curation, Writing - original draft. **Seyed Ahmad Alavi:** Supervision, Conceptualization, Investigation, Writing - review & editing. **Manuel Díaz-Azpiroz:** Conceptualization, Investigation, Visualization, Writing - review & editing. **Soheil Mohammadi:** Investigation, Software. **Mohammad Reza Ghassemi:** Conceptualization, Investigation, Writing - review & editing. **Carlos Fernández:** Conceptualization, Investigation, Visualization, Writing - review & editing. **Leticia Barcos:** Conceptualization, Investigation, Visualization, Writing - review & editing. **Marcel Frehner:** Conceptualization, Investigation, Writing - review & editing.

Acknowledgments

Seyed Tohid Nabavi thanks Prof. Jordi Carreras and Dr. Elena Druguet for their help, and constructive discussions on progressive deformation, shear zones, and transpressive settings during scientific field trips in the Cap de Creus, the Roses and the Axial Zone of Pyrenees during his research visit period in Spain. Moreover, Seyed Tohid Nabavi thanks Dr. Jonas B. Ruh for teaching and discussions on the finite difference method programming during his research visit period in the Institute of Earth Sciences “Jaume Almera” (CSIC-ICTJA), Barcelona, Spain. Manuel Díaz-Azpiroz and Carlos Fernández gratefully acknowledge financial support from the Spanish Ministry of Science, Innovation and University (projects PGC2018-100914-B-I00 and PGC2018-096534-B-I00). This work forms part of the Ph.D. thesis of Seyed Tohid Nabavi at Shahid Beheshti University, Tehran, Iran. We thank reviewers Prof. Fernando O. Marques and Prof. Soumyajit Mukherjee for constructive reviews, comments and helpful suggestions which allowed us to improve the original manuscript. Editorial and handling efforts by Prof. Ian Alsop are also gratefully acknowledged.

References

Alonso-Henar, J., Fernández, C., Martínez-Díaz, J.J., 2020. Application of the analytic model of general triclinic transpression with oblique extrusion to an active deformation zone: the Alhama de Murcia Fault (SE Iberian Peninsula). J. Struct. Geol. 130 https://doi.org/10.1016/j.jsg.2019.103924.

Alsop, G.I., Bryson, R., Hutton, D.H.W., 1998. Ductile transpression and localization of deformation along tectonic boundaries in the Caledonides of northwestern Ireland. Geol. Mag. 135, 699–718.

Alsop, G.I., Cheer, D.A., Strachan, R.A., Krabbendam, M., Kinny, P.D., Holdsworth, R.E., Leslie, A.G., 2010. Progressive fold and fabric evolution associated with regional strain gradients: a case study from across a Scandian ductile thrust nappe, Scottish Caledonides. In: Law, R.D., Butler, R.W.H., Holdsworth, R.E., Krabbendam, M., Strachan, R.A. (Eds.), Continental Tectonics and Mountain Building: the Legacy of Peach and Horne, vol. 335. Geological Society of London, Special Publications, pp. 255–274.

Balgord, E.A., Carrapa, B., 2016. Basin evolution of upper cretaceous-lower cenozoic strata in the Malargüe fold-and-thrust belt: northern Neuquén basin, Argentina. Basin Res. 28, 183–206.

Barcos, L., 2015. Combined Analytical and Analogue Modelling of Strongly Partitioned Transpression. The Torcal Shear Zone (External Betics). Ph.D. thesis. Universidad Pablo de Olavide, Sevilla, Spain.

Barcos, L., Díaz-Azpiroz, M., Expósito, I., 2011. Dominios estructurales y reparto de la deformación en zonas transpressivas de corteza superior (Torca de Antequera, Cadena Bética). Geogaceta 50, 31–34.

Barcos, L., Balanyá, J.C., Díaz-Azpiroz, M., Expósito, I., Jiménez-Bonilla, A., 2015. Kinematic of the torcal shear zone: transpressional tectonics in a salient-recess transition at the northern Gibraltar arc. Tectonophysics 663, 62–77.

Barcos, L., Díaz-Azpiroz, M., Balanyá, J.C., Expósito, I., Jiménez-Bonilla, A., Faccenna, C., 2016. Analogue modelling of inclined, brittle-ductile transpression: testing analytical models through natural shear zones (external Betics). Tectonophysics 682, 169–185.

Bergh, S.G., Sylvester, A.G., Damte, A., Indrevær, K., 2019. Polyphase kinematic history of transpression along the Mecca Hill segment of the San Andreas fault, southern California. Geosphere 15, 901–934.

Bieniawski, Z.T., 1984. Rock Mechanics Design in Mining and Tunneling (Boston, A.A. Balkema).

Boersma, Q.D., Douma, L.A.N.R., Bertotti, G., Barnhoorn, A., 2020. Mechanical controls on horizontal stresses and fracture behavior in layered rocks: a numerical sensitivity analysis. J. Struct. Geol. 130 https://doi.org/10.1016/j.jsg.2019.103907.

Bose, N., Mukherjee, S., 2019. Field documentation and genesis of back-structures in ductile and brittle regimes from the foreland part of a collisional orogen: examples from the Darjeeling-Sikkim Lesser Himalaya, India. Int. J. Earth Sci. 108, 1333–1350.

Bose, N., Dutta, D., Mukherjee, S., 2018. Role of grain-size in phyllonitisation: insights from mineralogy, microstructures, strain analysis and numerical modeling. J. Struct. Geol. 112, 39–52.

Bott, M.H.P., 1959. The mechanics of oblique slip faulting. Geol. Mag. 96, 109–117.

Bourne, S., 2003. Contrast of elastic properties between rock layers as a mechanism for the initiation and orientation of tensile failure under uniform remote compression. J. Geophys. Res. 108, 2395. https://doi.org/10.1029/2001JB001725.

Bowman, D., King, G., Tapponnier, P., 2003. Slip partitioning by elastoplastic propagation of oblique slip at depth. Science 300, 1121–1123.

Bradley, K.E., Feng, L., Hill, E.M., Natawidjaja, D.H., Sieh, K., 2017. Implications of the diffuse deformation of the Indian Ocean lithosphere for slip partitioning of oblique plate convergence in Sumatra. J. Geophys. Res.: Solid Earth 122, 572–591.

Brandes, C., Tanner, D.C., 2014. Fault-related folding: a review of kinematic models and their application. Earth Sci. Rev. 138, 352–370.

Braun, J., Beaumont, C., 1995. Three dimensional numerical experiments of strain partitioning at oblique plate boundaries: implications for contrasting tectonic styles in the southern Coast Ranges, California, and central South Island, New Zealand. J. Geophys. Res. 100, 18059–18074.

Burbidge, D.R., Braun, J., 1998. Analogue models of obliquely convergent continental plate boundaries. J. Geophys. Res. 103, 15221–15237.

Burberry, C.M., 2015. Spatial and temporal variation in penetrative strain during compression: insights from analog models. Lithosphere 7, 611–624.

Byerlee, J.D., 1970. The mechanics of stick-slip. Tectonophysics 9, 475–486.

Calignano, E., Sokoutis, D., Willingshofer, E., Brun, J.-P., Gueydan, F., Cloetingh, S., 2017. Oblique contractional reactivation of inherited heterogeneities: cause for arcuate orogens. Tectonics 36, 542–558.

Carmichael, R.S., 1982. Handbook of Physical Properties of Rocks, vol. 2. Chemical Rubber Company Press, Boca Raton, Florida.

Carreras, J., Cosgrove, J.W., Druguet, E., 2013. Strain partitioning in banded and/or anisotropic rocks: implications for inferring tectonic regimes. J. Struct. Geol. 50, 7–21.

Carreras, J., Druguet, E., 2019. Complex fold patterns developed by progressive deformation. J. Struct. Geol. 125, 195–201.

Casas, A.M., Gapais, D., Naplas, T., Besnard, K., Román-Berdiel, T., 2001. Analogue models of transpressive systems. J. Struct. Geol. 23, 733–743.

Casini, G., Romaire, I., Casciello, E., Saura, E., Vergés, J., Fernández, N., Hunt, D.W., 2018. Fracture characterization in sigmoidal folds: insights from the siah Kuh anticline, Zagros, Iran. AAPG (Am. Assoc. Pet. Geol.) Bull. 102, 369–399.

Cooke, M., Underwood, C., 2001. Fracture termination and step-over at bedding interfaces due to frictional slip and interface opening. J. Struct. Geol. 23, 223–238.

Crespo-Blanc, A., Jiménez-Bonilla, A., Balanyá, J.C., Expósito, I., Díaz-Azpiroz, M., 2018. From field data to lithospheric-scale models going through analogue experiments: the Gibraltar Arc system revisited in the light of the external zones structural evolution. Rev. Soc. Geol. Espana 31, 111–122.

Cruz, L., Teyssier, C., Perg, L., Take, A., Fayon, A., 2008. Deformation, exhumation, and topography of experimental doubly-vergent orogenic wedges subjected to asymmetric erosion. J. Struct. Geol. 30, 98–115.

Curtis, M.L., 1998. Development of kinematic partitioning within a pure-shear dominated dextral transpression zone: the southern Ellsworth Mountains, Antarctica. In: Holdsworth, R.E., Strachan, R.A., Dewey, J.F. (Eds.), Continental Transpressional and Transtensional Tectonics, vol. 135. Geological Society of London, Special Publications, pp. 289–306.

Czeck, D.M., Hudleston, P.J., 2003. Testing models for obliquely plunging lineations in transpression: a natural example and theoretical discussion. J. Struct. Geol. 25, 959–982.

Czeck, D.M., Hudleston, P.J., 2004. Physical experiments of vertical transpression with localized nonvertical extrusion. J. Struct. Geol. 26, 573–581.
Dasgupta, S., Mandal, N., Bose, S., 2015. How far does a ductile shear zone permit transpression? In: Mukherjee, S., Mulchrone, K.F. (Eds.), Ductile Shear Zones: from Micro- to Macro-Scales. Springer, pp. 14–29.
Davis, J.R., Titus, S.J., 2011. Homogenous steady deformation: a review of computational techniques. J. Struct. Geol. 33, 1046–1062.
Davis, J.R., Titus, S.J., Horsman, E., 2013. Non-steady homogeneous deformations: computational techniques using Lie theory, and application to ellipsoidal markers in naturally deformed rocks. J. Struct. Geol. 56, 142–155.
Derikvand, B., Alavi, S.A., Abdollahie Fard, I., Hajialibeigi, H., 2018. Folding style of the Dezful Embayment of Zagros Belt: signature of detachment horizons, deep-rooted faulting and syn-deformation deposition. Mar. Petrol. Geol. 91, 501–518.
Dewey, J.F., Holdsworth, R.E., Strachan, R.A., 1998. Transpression and transtension zones. In: Holdsworth, R.E., Strachan, R.A., Dewey, J.F. (Eds.), Continental Transpressional and Transtensional Tectonics, vol. 135. Geological Society of London, Special Publications, pp. 1–14.
Díaz-Azpiroz, M., Fernández, C., 2005. Kinematic analysis of the southern Iberian shear zone and tectonic evolution of the Acebuches metabasites (SW Variscan Iberian Massif). Tectonics 24 (3). https://doi.org/10.1029/2004TC001682.
Díaz-Azpiroz, M., Barcos, L., Balanyá, J.C., Fernández, C., Expósito, I., Czeck, D.M., 2014. Applying a general triclinic transpression model to highly partitioned brittle-ductile shear zones: a case study from the Torcal de Antequera massif, external Betics, southern Spain. J. Struct. Geol. 68, 316–336.
Díaz-Azpiroz, M., Brune, S., Leever, K.A., Fernández, C., Czeck, D.M., 2016. Tectonics of oblique plate boundary systems. Tectonophysics 693, 165–170.
Díaz-Azpiroz, M., Fernández, C., Czeck, D.M., 2019. Are we studying deformed rocks in the right sections? Best practices in the kinematic analysis of 3D deformation zones. J. Struct. Geol. 125, 218–225.
Druguet, E., Alsop, G.I., Carreras, J., 2009. Coeval brittle and ductile structures associated with extreme deformation partitioning in a multilayer sequence. J. Struct. Geol. 31, 498–511.
Dutton, B.J., 1997. Finite strains in transpression zones with no boundary slip. J. Struct. Geol. 19, 1189–1200.
England, P., 1989. Large rates of rotation in continental lithosphere undergoing distributed deformation. In: Kissel, C., Laj, C. (Eds.), Paleomagnetic Rotation and Continental Deformation. Kluwer, Dordrecht, pp. 157–164.
Eschbac, O.W., 1961. Handbook of Engineering Fundamentals, Handbook Series. John Wiley and Sons, New York.
Fedorik, J., Zwaan, F., Schreurs, G., Toscani, G., Bonini, L., Seno, S., 2019. The interaction between strike-slip dominated fault zones and thrust belt structures: insights from 4D analogue models. J. Struct. Geol. 122, 89–105.
Fernández, C., Díaz-Azpiroz, M., 2009. Triclinic transpression zones with inclined extrusion. J. Struct. Geol. 31, 1255–1269.
Fernández, C., Czeck, D.M., Díaz-Azpiroz, M., 2013. Testing the model of oblique transpression with oblique extrusion in two natural cases: steps and consequences. J. Struct. Geol. 54, 85–102.
Ferrill, D.A., Morris, A.P., 2008. Fault zone deformation controlled by carbonate mechanical stratigraphy, Balcones fault system, Texas. AAPG (Am. Assoc. Pet. Geol.) Bull. 92, 359–380.
Ferrill, D.A., Morris, A.P., McGinnis, R.N., Smart, K.J., Wigginton, S.S., Hill, N.J., 2017. Mechanical stratigraphy and normal faulting. J. Struct. Geol. 94, 275–302.
Fossen, H., Tikoff, B., 1993. The deformation matrix for simultaneous simple shearing, pure shearing and volume change, and its application to transpression-transtension tectonics. J. Struct. Geol. 15, 413–422.
Fossen, H., Tikoff, B., Teyssier, C., 1994. Strain modelling of transpressional and transtensional deformation. Nor. Geol. Tidsskr. 74, 134–145.
Fossen, H., Tikoff, B., 1998. Extended models of transpression and transtension, and application to tectonic settings. In: Holdsworth, R.E., Strachan, R.A., Dewey, J.F. (Eds.), Continental Transpressional and Transtensional Tectonics, vol. 135. Geological Society of London, Special Publications, pp. 15–33.
Fossen, H., Teyssier, C., Whitney, D.L., 2013. Transtensional folding. J. Struct. Geol. 56, 89–102.
Fossen, H., Cavalcante, G.C.G., 2017. Shear zones – a review. Earth Sci. Rev. 171, 434–455.
Fossen, H., Cavalcante, G.C.G., Pinheiro, R.V.L., Archanjo, C.J., 2019. Deformation – progressive or multiphase? J. Struct. Geol. 125, 82–99.
Frehner, M., 2014. 3D fold growth rates. Terra. Nova 26, 417–424.
Frehner, M., 2016. 3D fold growth in transpression. Tectononphysics 693, 183–196.
Ghosh, N., Chakra, M., Chattopadhyay, A., 2014. An experimental approach to strain pattern and folding in unconfined and/or partitioned transpressional deformation. Int. J. Earth Sci. 103, 349–365.
Gomez-Rivas, E., Griera, A., 2012. Shear fractures in anisotropic ductile materials: an experimental approach. J. Struct. Geol. 34, 61–76.
Graveleau, F., Malavieille, J., Dominguez, S., 2012. Experimental modelling of orogenic wedges: a review. Tectonophysics 538–540, 1–66.
Harland, W.B., 1971. Tectonic transpression in caledonian spitsbergen. Geol. Mag. 108, 27–42.
Holdsworth, R.E., Stewart, M., Imber, J., Strachan, R.A., 2001. The structure and rheological evolution of reactivated continental fault zones: a review and case study. In: Miller, J.A., Holdsworth, R.E., Buick, I.S., Hand, M. (Eds.), Continental Reactivation and Reworking, vol. 184. Geological Society of London, Special Publications, pp. 115–137.
Horsman, E., Tikoff, B., Czeck, D., 2008. Rheological implications of heterogeneous deformation at multiple scales in the Late Cretaceous Sierra Nevada, California. Geol. Soc. Am. Bull. 120, 238–255.
Hudleston, P.J., Schultz-Ela, D., Southwick, D.L., 1988. Transpression in an Archean greenstone belt, northern Minnesota. Can. J. Earth Sci. 25, 1060–1068.
Hughes, A.N., Benesh, N.P., Shaw, J.H., 2014. Factors that control the development of fault-bend versus fault-propagation folds: insights from mechanical models based on the discrete element method (DEM). J. Struct. Geol. 68, 121–141.
Hughes, A.N., Shaw, J.H., 2015. Insights into the mechanics of fault-propagation folding styles. Geol. Soc. Am. Bull. 127 (11–12), 1752–1765.
Iacopini, D., Passchier, C.W., Koehn, D., Carosi, R., 2007. Fabric attractors in general triclinic glow systems and their application to high strain shear zones: a dynamical systems approach. J. Struct. Geol. 29, 298–317.
Jaeger, J.C., Cook, N.G.W., Zimmerman, R.W., 2007. Fundamental of Rock Mechanics, fourth ed. Blackwell, Malden.
Jiang, D., 2007. Sustainable transpression: an examination of strain and kinematics in deforming zones with migrating boundaries. J. Struct. Geol. 29, 1984–2005.
Jiang, D., Bentley, C., 2012. A micromechanical approach for simulating multiscale fabrics in large-scale high-strain zones: theory and application. J. Geophys. Res. 117 https://doi.org/10.1029/2012JB009327.
Jones, R.R., Tanner, P.W.G., 1995. Strain partitioning in transpression zones. J. Struct. Geol. 17, 793–802.
Jones, R.R., Holdsworth, R.E., Clegg, P., McCaffrey, K., Tavarnelli, E., 2004. Inclined transpression. J. Struct. Geol. 26, 1531–1548.
Jones, R.R., Holdsworth, R.E., McCaffrey, K., Clegg, P., Tavarnelli, E., 2005. Scale dependence, strain compatibility and heterogeneity of three-dimensional deformation during mountain building: a discussion. J. Struct. Geol. 27, 1190–1204.
Koyi, H.A., Maillot, B., 2007. Tectonic thickening of hanging-wall units over a ramp. J. Struct. Geol. 29, 924–932.
Leever, K.A., Gabrielsen, R.H., Sokoutis, D., Willingshofer, E., 2011. The effect of convergence angle on the kinematic evolution of strain partitioning in transpressional brittle wedges: insights from analog modeling and high-resolution digital image analysis. Tectonics 30, TC2013. https://doi.org/10.1029/2010TC002823.
Li, Z., Zhang, P., Zheng, W., Jia, D., Hubbard, J., Almeida, R., Sun, C., Shi, X., Li, T., 2018. Oblique thrusting and strain partitioning in the Longmen Shan fold-and-thrust belt, eastern Tibetan Plateau. J. Geophys. Res.: Solid Earth 123, 4431–4453.
Lin, S., Jiang, D., Williams, P.F., 1998. Transpression (or transtension) zones of triclinic symmetry; natural example and theoretical modelling. In: Holdsworth, R.E., Strachan, R.A., Dewey, J.F. (Eds.), Continental Transpressional and Transtensional Tectonics, vol. 135. Geological Society of London, Special Publications, pp. 41–57.
Malavieille, J., Dominguez, S., Lu, C.-Y., Chen, C.-T., Konstantinovskaya, E., 2019. Deformation partitioning in mountain belts: insights from analogue modelling experiments and the Taiwan collisional orogeny. Geol. Mag. https://doi.org/10.1017/S0016756819000645.
Malz, A., Madritsch, H., Meier, B., Kley, J., 2016. An unusual triangle zone in the external northern Alpine foreland (Switzerland): structural inheritance, kinematics and implications for the development of the adjacent Jura fold-and-thrust belt. Tectonophysics 670, 127–143.
Marques, F.O., Nogueira, C.R., 2008. Normal fault inversion by orthogonal compression: sandbox experiments with weak faults. J. Struct. Geol. 30, 761–766.
Marques, F.O., Ranalli, G., Mandal, N., 2018a. Tectonic overpressure at shallow depth in the lithosphere: the effects of boundary conditions. Tectonophysics 746, 702–715.
Marques, F.O., Mandal, N., Ghosh, S., Ranalli, G., Bose, S., 2018b. Channel flow, tectonic overpressure, and exhumation of high-pressure rocks in the Greater Himalayas. Solid Earth 9, 1061–1078.
McClay, K.R., Buchanan, P.G., 1992. Thrust faults in inverted extensional basins. In: McClay, K.R. (Ed.), Thrust Tectonics, pp. 93–104.
McClay, K.R., Whitehouse, P.S., Dooley, T., Richards, M., 2004. 3D evolution of fold and thrust belts formed by oblique convergence. Mar. Petrol. Geol. 21, 857–877.
McGinnis, R.N., Ferrill, D.A., Morris, A.P., Smart, K.J., 2016. Insight on mechanical stratigraphy and subsurface interpretation. In: Krantz, B., Ormand, C., Freeman, B. (Eds.), 3-D Structural Interpretation: Earth, Mind, and Machine, vol. 111. American Association of Petroleum Geologists Memoir, pp. 111–120.
McKenzie, D., Jackson, J., 1986. A block model of distributed deformation by faulting. J. Geol. Soc. (Lond.) 143, 349–353. London.
Michie, E.A.H., Haines, T.J., Healy, D., Neilson, J.E., Timms, N.E., Wibberley, C.A.J., 2014. Influence of carbonate facies on fault zone architecture. J. Struct. Geol. 65, 82–99.
Molnar, P., Taponnier, P., 1975. Cenozoic tectonics of Asia: effects of a continental collision. Science 198, 419–426.
Morris, A., Ferrill, D.A., Henderson, D.B., 1996. Slip-tendency analysis and fault reactivation. Geology 24, 275–278.
Morris, A.P., Ferrill, D.A., McGinnis, R.N., 2016. Using fault displacement and slip tendency to estimate stress states. J. Struct. Geol. 83, 60–72.
Mukherjee, S., 2013. Channel flow extrusion model to constrain dynamic viscosity and Prandtl number of the Higher Himalayan Shear Zone. Int. J. Earth Sci. 102, 1811–1835.
Mukherjee, S., Koyi, H.A., 2010. Higher Himalayan Shear Zone, Sutlej section: structural geology and extrusion mechanism by various combinations of simple shear, pure shear and channel flow in shifting modes. Int. J. Earth Sci. 99, 1267–1303.
Mukherjee, S., Koyi, H.A., Talbot, C.J., 2012. Implication of channel flow analogue models for extrusion of the Higher Himalayan Shear Zone with special reference to the out-of-sequence thrusting. Int. J. Earth Sci. 101, 253–272.
Nabavi, S.T., Alavi, S.A., Mohammadi, S., Ghassemi, M.R., Frehner, M., 2017a. Analysis of transpression within contractional fault steps using finite-element method. J. Struct. Geol. 96, 1–20.
Nabavi, S.T., Díaz-Azpiroz, M., Talbot, C.J., 2017b. Inclined transpression in the neka valley, eastern Alborz, Iran. Int. J. Earth Sci. 106, 1815–1840.

Nabavi, S.T., Rahimi-Chakdel, A., Khademi, M., 2017c. Structural pattern and emplacement mechanism of the Neka Valley nappe complex, eastern Alborz, Iran. Int. J. Earth Sci. 106, 2387–2405.
Nabavi, S.T., Alavi, S.A., Mohammadi, S., Ghassemi, M.R., 2018a. Mechanical evolution of transpression zones affected by fault interactions: insights from 3D elasto-plastic finite element models. J. Struct. Geol. 106, 19–40.
Nabavi, S.T., Alavi, S.A., Maerten, F., 2018b. 2D finite-element elastic models of transtensional pull-apart basins. Compt. Rendus Geosci. 350, 222–230.
Nabavi, S.T., Alavi, S.A., Javanbakht, J.H., 2019. The Dinevar trantensional pull-apart basin, NW Zagros Mountains, Iran: a geological study and comparison to 2D finite element elastic models. Int. J. Earth Sci. 108, 329–346.
Nevitt, J.M., Pollard, D.D., Warren, J.M., 2014. Evaluation of transtension and transpression within contractional fault steps: comparing kinematic and mechanical models to field data. J. Struct. Geol. 60, 55–69.
Nevitt, J.M., Warren, J.M., Pollard, D.D., 2017. Testing constitutive equations for brittle-ductile deformation associated with faulting in granitic rock. J. Geophys. Res.: Solid Earth 122, 6269–6293.
Nussbaum, C., Kloppenburg, A., Caër, T., Bossart, P., 2017. Tectonic evolution around the Mont Terri rock laboratory, northwestern Swiss Jura: constraints from kinematic forward modelling. Swiss J. Geosci. 110, 39–66.
Peacock, D.C.P., Dimmen, V., Rotevatn, A., Sanderson, D.J., 2017. A boarder classification of damage zones. J. Struct. Geol. 102, 179–192.
Philippon, M., Corti, G., 2016. Obliquity along plate boundaries. Tectonophysics 693, 171–182.
Pollard, D.D., Fletcher, R.C., 2005. Fundamental of Structural Geology. Cambridge University Press.
Powell, C.M., 1987. Inversion tectonics in S.W. Dyfed. Proc. Geologists' Assoc. 98 (3), 193–203.
Ratschbacher, L., Merle, O., Davy, P., Cobbold, P.R., 1991. Lateral extrusion in the eastern Alps, Part 1: boundary conditions and experiments scaled for gravity. Tectonics 10, 245–256.
Richard, P., Cobbold, P.R., 1990. Experimental insights into partitioning of fault motions in continental convergent wrench zones. Ann. Tect. 4, 35–44.
Robin, P.-Y.F., Cruden, A.R., 1994. Strain and vorticity patterns in ideally ductile transpression zones. J. Struct. Geol. 4, 447–466.
Rosas, F.M., Duarte, J.C., Almeida, P., Schellart, W.P., Riel, N., Terrinha, P., 2017. Analogue modelling of thrust systems: passive vs. active hanging wall strain accommodation and sharp vs. smooth fault-ramp geometries. J. Struct. Geol. 99, 45–69.
Ruh, J.B., Kaus, B.J.P., Burg, J.-P., 2012. Numerical investigation of deformation mechanics in fold-and-thrust belts: influence of rheology of single and multiple décollements. Tectonics 31, TC3005. https://doi.org/10.1029/2011TC003047.
Ruh, J.B., Gerya, T., Burg, J.-P., 2014. 3D effects of strain vs. velocity weakening on deformation patterns in accretionary wedges. Tectonophysics 615–616, 122–141.
Ruh, J.B., Gerya, T., Burg, J.-P., 2017. Toward 4D modeling of orogenic belts: example from the transpressive Zagros Fold Belt. Tectonophysics 702, 82–89.
Sadeghi, S., Storti, F., Yassaghi, A., Nestola, Y., Cavozzi, C., 2016. Experimental deformation partitioning in obliquely converging orogens with lateral variation of basal décollement rheology: influences for NW Zagros, Iran. Tectonophysics 693, 223–238.
Sançar, T., Zabcı, C., Akyüz, H.S., Sunal, G., Villa, I.M., 2015. Distributed transpressive continental deformation: the Varto Fault Zone, eastern Turkey. Tectonophysics 661, 99–111.
Sanderson, D.J., Marchini, W.R.D., 1984. Transpression. J. Struct. Geol. 6, 449–458.
Sarkarinejad, K., Godin, L., Faghih, A., 2009. Kinematic vorticity flow analysis and $^{40}Ar/^{39}Ar$ geochronology related to inclined extrusion of the HP-LT metamorphic rocks along the Zagros accretionary prism, Iran. J. Struct. Geol. 31, 691–706.
Sarkarinejad, K., Razavi Pash, R., Motamedi, H., Yazdani, M., 2018. Deformation and kinematic evolution of the subsurface structures: Zagros foreland fold-and-thrust belt, northern Dezful Embayment, Iran. Int. J. Earth Sci. 107, 1287–1304.
Sarkarinejad, K., Partabian, A., Faghih, A., 2013. Variation in the kinematics of deformation along the Zagros inclined transpression zone, Iran: implications for defining a curved inclined transpression zone. J. Struct. Geol. 48, 126–136.
Schreurs, G., 2003. Fault development and interaction in distributed strike-slip shear zones: an experimental approach. In: Storti, F., Holdsworth, R.E., Salvini, F. (Eds.), Intraplate Strike-Slip Deformation Belts, vol. 210. Geological Society of London, Special Publications, pp. 35–52.
Schreurs, G., Colletta, B., 1998. Analogue modelling of faulting in zones of continental transpression and transtension. In: Holdsworth, R.E., Strachan, R.A., Dewey, J.F. (Eds.), Continental Transpressional and Transtensional Tectonics, vol. 135. Geological Society of London, Special Publications, pp. 59–79.
Schreurs, G., Colletta, B., 2002. Analogue modelling of continental transpression. In: Schellart, W.P., Passchier, W.P. (Eds.), Analogue Modelling of Large-Scale Tectonic Processes. Journal of Virtual Explorer, vol. 7, pp. 103–114.
Schulmann, K., Gayer, R., 2000. A model for a continental accretionary wedge developed by oblique collision: the NE Bohemian Massif. J. Geol. Soc. 157, 401–416. London.
Schulmann, K., Thompson, A.B., Lexa, O., Ježek, J., 2003. Strain distribution and fabric development modeled in active and ancient transpressive zones. J. Geophys. Res. 108 https://doi.org/10.1029/2001JBooo632. ETG 6-1-ETG 6-15.
Simonetti, M., Carosi, R., Montomoli, C., Langone, A., D'Addario, E., Mammoliti, E., 2018. Kinematic and geochronological constraints on shear deformation in the Ferriere-Mollières shear zone (Argentera-Mercantour massif, western Alps): implications for the evolution of the southern European variscan belt. Int. J. Earth Sci. 107, 2163–2189.
Stephens, T.L., Walker, R.J., Healy, D., Bubeck, A., England, R.W., McCaffrey, K.J.W., 2017. Igneous sills record far-field and near field stress interactions during volcano construction: Isle of Mull, Scotland. Earth Planet Sci. Lett. 478, 159–174.
Sullivan, W.A., Law, R.D., 2007. Deformation path partitioning within the transpressional White Mountain shear zone, California and Nevada. J. Struct. Geol. 29, 583–598.
Tavarnelli, E., Holdsworth, R.E., Clegg, P., Jones, R.R., McCaffrey, K.J.W., 2004. The anatomy and evolution of a transpressional imbricate zone, Southern Uplands, Scotland. J. Struct. Geol. 26, 1341–1360.
Tikoff, B., Teyssier, C., 1994. Strain modeling of displacement-field partitioning in transpressional orogens. J. Struct. Geol. 16, 1575–1588.
Tikoff, B., Peterson, K., 1998. Physical experiments of transpressional folding. J. Struct. Geol. 20, 661–672.
Titus, S.J., Housen, B., Tikoff, B., 2007. A kinematic model for the Rinconada fault system in central California based on structural analysis of en echelon folds and paleomagnetism. J. Struct. Geol. 29, 961–982.
Toy, V.G., Norris, R.J., Prior, D.J., Walrond, M., Cooper, A.F., 2013. How do lineations reflect the strain history of transpressive shear zones? The example of the active Alpine Fault Zone, New Zealand. J. Struct. Geol. 50, 187–198.
Treagus, S.H., 1993. Flow variations in power-law multilayers: implications for competence contrasts in rocks. J. Struct. Geol. 15, 423–434.
van Gelder, I.E., Willingshofer, E., Sokoutis, D., Cloetingh, S.A.P.L., 2017. The interplay between subduction and lateral extrusion: a case study for the European Easter Alps based on analogue models. Earth Planet Sci. Lett. 472, 82–94.
Viola, G., Henderson, I.C., 2010. Inclined transpression at the toe of an arcuate thrust: an example from the Precambrian 'Mylonite Zone' of the Sveconorwegian orogen. In: Law, R.D., Butler, R.W.H., Holdsworth, R.E., Krabbendam, M., Strachan, R.A. (Eds.), Continental Tectonics and Mountain Building: the Legacy of Peach and Horne, vol. 335. Geological Society of London, Special Publications, pp. 715–737.
Vitale, S., Mazzoli, S., 2008. Heterogeneous shear zone evolution: the role of shear strain hardening/softening. J. Struct. Geol. 30, 1383–1395.
Vitale, S., Mazzoli, S., 2015. From finite to incremental strain: insights into heterogeneous shear zone evolution. In: Mukherjee, S., Mulchrone, K.F. (Eds.), Kinematics of Ductile Shear Zones in Meso- and Micro-scales. Wiley and Blackwell, pp. 3–13.
von Tscharner, M., Schmalholz, S.M., Epard, J.-L., 2016. 3-D numerical models of viscous flow applied to fold nappes and the Rawil depression in the Helvetic nappe system (western Switzerland). J. Struct. Geol. 86, 32–46.
Woodward, N.B., Rutherford Jr., E., 1989. Structural lithic units in external orogenic zones. Tectonophysics 158, 247–267.
Xypolias, P., Gerogiannis, N., Chatzaras, V., Papapavlou, K., Kruckenberg, S.C., Aravadinou, E., Miches, Z., 2018. Using incremental elongation and shearing to unravel the kinematics of a complex transpressional zone. J. Struct. Geol. 115, 64–81.
Xu, S., Fukuyama, E., Ben-Zion, Y., Ampuero, J.-P., 2015. Dynamic rupture activation of backthrust fault branching. Tectonophysics 644–645, 161–183.
Zanchi, A., Zanchetta, S., Balini, M., Ghassemi, M.R., 2016. Oblique convergence during the cimmerian collision: evidence from the triassic Aghdarband basin, NE Iran. Godwana Res. 38, 149–170.
Ziesch, J., Tanner, D.C., Krawczyk, C.M., 2014. Strain associated with the fault-parallel flow algorithm during kinematic fault displacement. Math. Geosci. 46 (1), 59–73.